MXENES AS FLOW ELECTRODES FOR CAPACITIVE DEIONIZATION OF

WASTEWATER


by

Naqsh E. Mansoor


A thesis

submitted in partial fulfillment

of the requirements for the degree of

Master of Science in Materials Science & Engineering

Boise State University


August 2020

BOISE STATE UNIVERSITY GRADUATE COLLEGE

## DEFENSE COMMITTEE AND FINAL READING APPROVALS

of the thesis submitted by

Naqsh E. Mansoor

Thesis Title:    MXenes as Flow Electrodes for Capacitive Deionization of Wastewater

Date of Final Oral Examination:              25 June 2020

The following individuals read and discussed the thesis submitted by student Naqsh E. Mansoor, and they evaluated their presentation and response to questions during the final oral examination. They found that the student passed the final oral examination.

David Estrada, Ph.D.                          Chair, Supervisory Committee

Brian Jaques, Ph.D.                           Member, Supervisory Committee

Paul Simmonds, Ph.D.                          Member, Supervisory Committee

Harish Subbaraman, Ph.D.                      Member, Supervisory Committee

The final reading approval of the thesis was granted by David Estrada, Ph.D., Chair of the Supervisory Committee. The thesis was approved by the Graduate College.

DEDICATION


For all the women in science who paved the way so that I could be here today.

We stand on the shoulders of giants.

ACKNOWLEDGMENTS

ABSTRACT

The energy-water nexus poses an integrated research challenge, while opening up an opportunity space for the development of energy efficient technologies for water remediation. Capacitive Deionization (CDI) is an upcoming reclamation technology that uses a small applied voltage applied across electrodes to *electrophoretically* remove dissolved ionic impurities from wastewater streams. Similar to a supercapacitor, the ions are stored in the electric double layer of the electrodes. Reversing the polarity of applied voltage enables recovery of the removed ionic impurities, allowing for recycling and reuse. Simultaneous materials recovery and water reclamation makes CDI energy efficient and resource conservative, with potential to scale it up for industrial applications. The efficiency of the technology depends on the architectural design of the CDI cell, control of operating conditions, and the nature of the electrodes used. In this project we report on the performance of $Ti_3C_2T_x$ MXenes flow electrodes in a CDI cell design. MXenes are a novel class of two-dimensional (2D) transition metal carbides, nitrides and carbonitrides with the general formula $M_{n+1}X_nT_x$ where M is an early transition metal, X is carbon and/or nitrogen, $T_x$ represents the surface terminations. $Ti_3C_2T_x$ MXenes synthesized at Boise State, were employed as a flow electrode solution in an established CDI cell for targeted and selective ion removal. Performance metrics of achieved a*dsorption capacity, ion removal efficiency, regeneration efficiency, energy consumption,* and *charge efficiency,* exceed those of currently prevalent electrode systems. In addition, rheological properties of the $Ti_3C_2T_x$ MXenes colloidal solution were evaluated. This work establishes the

deionization performance of $Ti_3C_2T_x$ MXene based flow electrodes while providing further insight towards understanding the effect of structure and surface functionalization on the resultant deionization efficiency.

TABLE OF CONTENTS

# LIST OF TABLES

LIST OF FIGURES

## LIST OF ABBREVIATIONS

| | |
|---|---|
| MSMSE | Micron School of Materials Science and Engineering |
| ANML | Advanced Nanomaterials and Manufacturing Laboratory |
| INL | Idaho National Laboratory |
| LDRD | Laboratory Directed Research and Development |
| R&D | Research & Development |
| CDI | Capacitive Deionization |
| MCDI | Membrane Capacitive Deionization |
| FE-CDI | Flow Electrode Capacitive Deionization |
| DOE | Department of Energy |
| IEA | International Energy Agency |
| EPA | Environmental Protection Agency |
| CWA | Clean Water Act |
| RO | Reverse Osmosis |
| 2D | Two-Dimensional |
| AC | Activated Carbon |
| BM | Match Mode |
| SP | Single Pass |
| DE | Dynamic Equilibrium |
| FL | Few Layer |
| ML | Multi Layer |

| | |
|---|---|
| PTFE | Polytetrafluoroethylene |
| MILD | Minimally Intensive Layer Delamination |
| RTP | Room Temperature and Pressure |
| XRD | X-Ray Diffraction |
| SEM | Scanning Electron Microscope |
| TEM | Transmission Electron Microscope |
| DI | Deionized |
| DLS | Dynamic Light Scattering |
| UV-Vis | Ultraviolet Visible |
| $\Gamma$ | Deionization Capacity |
| $\Lambda$ | Charge Efficiency |
| $\eta_{coul}$ | Coulumbic Efficiency Loss |
| $\eta_r$ | Electrode Regeneration Efficiency |
| $\zeta$ | Zeta |

CHAPTER ONE: INTRODUCTION

## 1.1     Motivation

Originating in the Himalayan Plateau, the mighty Indus River and its tributaries are the lifelines of my home country, Pakistan.  The region is primarily an agrarian economy [1]. The water quality in the Indus river basin has a direct impact on national food and economic security [2]. Similarly, the U.S. food system is one of the pillars of the U.S. economy. Food and agriculture industries contributed $1.053 trillion to the nation's gross domestic product (GDP) in 2017 alone [3]. The state of Idaho's economy is also heavily agriculture reliant. Agricultural production accounts for nearly 20% of the state's annual gross state product [4]. However, this productivity comes at an environmental cost. According to the U.S. Environmental Protection Agency (EPA), agriculture is the primary contributor to rising lake and river pollution [5]. Agricultural runoff is often the cause of water quality issues. It is typically loaded with phosphorous, ammonia, and nitrates due to animal waste and abundant use of fertilizers [6]. Orthodox agricultural practices lead to agricultural runoff accumulating in natural water sources, reducing water quality and disrupting aquatic ecosystems.

To ensure food and economic security, it is therefore imperative that agricultural waste is curtailed, and/or pre-treated before releasing into natural environments. Since most of agricultural waste is in the form of wastewater runoffs, the efficient pre-treatment of nutrient laden wastewater is a pressing research challenge.

## 1.2.    Research Goals

Currently prevalent agricultural wastewater treatment technologies are physical or biological in nature [7]. The practices within the industry primarily focus on pollutant mitigation to abide by the Clean Water Act (CWA) [8]. While there have been some efforts to reclaim and reuse agricultural wastewaters, the area remains largely untapped. There are no industrially widespread practices that simultaneously account for nutrient recovery alongside wastewater reclamation. This is a cause of concern as agricultural wastewaters are often laden with valuable nutrients, including but not limited to ammonia and nitrates. On the flip side, recovery technologies are often limited to being some variation of physical or chemical filtration, which is both time and resource-intensive. Hence, the wide aim of this project was the development of a resource and energy conservative technique that can target nutrient recovery alongside water reclamation. Extensive literature review revealed that capacitive deionization is an emerging technique that fits our widespread research goals, and was hence the area of focus in this project. This is further discussed in Chapter 2.

CHAPTER TWO: BACKGROUND

## 2.1. Capacitive Deionization

The concept of Capacitive Deionization (CDI) was first brought to light in the early 1960s [9]. The proof of concept paper by Blair and Murphy outlined the application of low voltage to electrophoretically remove dissolved ions from brackish water. However, the limited availability of high surface area, electrically conductive materials halted the progress of technology. The physical isolation of graphene in 2004 by Konstantin Novoselov and Andre Geim [10] led to a vigorous interest in carbon materials within the scientific community. Carbon in its various forms, including but not limited to graphite, carbon aerogels, carbon nanotubes, and graphene exhibit an unusual combination of attractive properties like high surface area, high electrical conductivity, surface sensitivity, and good mechanical strength [11]. Owing to these properties, research in carbon-based electrode materials piqued. Unsurprisingly, the first patent for membrane CDI (MCDI) was filed later in 2004 by Andelman and Walker [12]. This leads evidence to the fact that the development and progress of CDI technology is heavily reliant on the availability of suitable electrode materials.

A CDI system consists of an oppositely charged pair of porous electrodes that trap and store dissolved ions upon the application of an electrical voltage. Capacitive adsorption of ions is the primary mode of separation. This allows it to operate at voltages below the reduction potential of water (1.23 V), resulting in very low energy consumption. This is in direct contrast with technologies that involve chemical reactions [13]. The system operates

in two steps which are shown schematically in Fig. 2.1. [14]. The *charging* step involves

the application of electrical voltage for the harvesting and storage of ions to yield purified,

deionized water. The *discharging* step involves the switching of applied voltage polarity

following the saturation of electrodes. This releases the adsorbed ions, which are collected

in a separate concentrated stream. This makes CDI optimal for not only removal but also

recovery of dissolved nutrients.
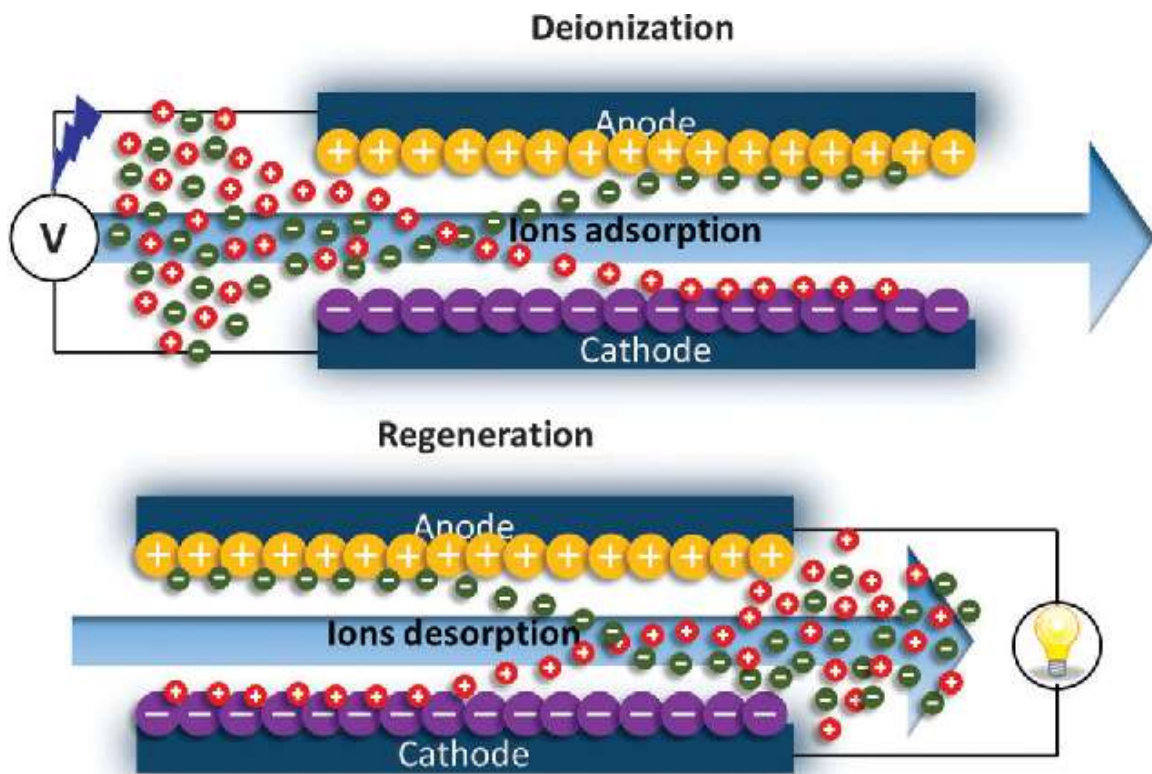


**Figure  2.1.    Schematic representation of the CDI process [14].**

Flow-by CDI, as represented in Fig. 2.1. is the quintessential CDI setup. However, since

its inception in the early 1960s, many different cell architectures have been explored. The

timeline for the development of various cell architectures is shown in Fig. 2.2. [15].
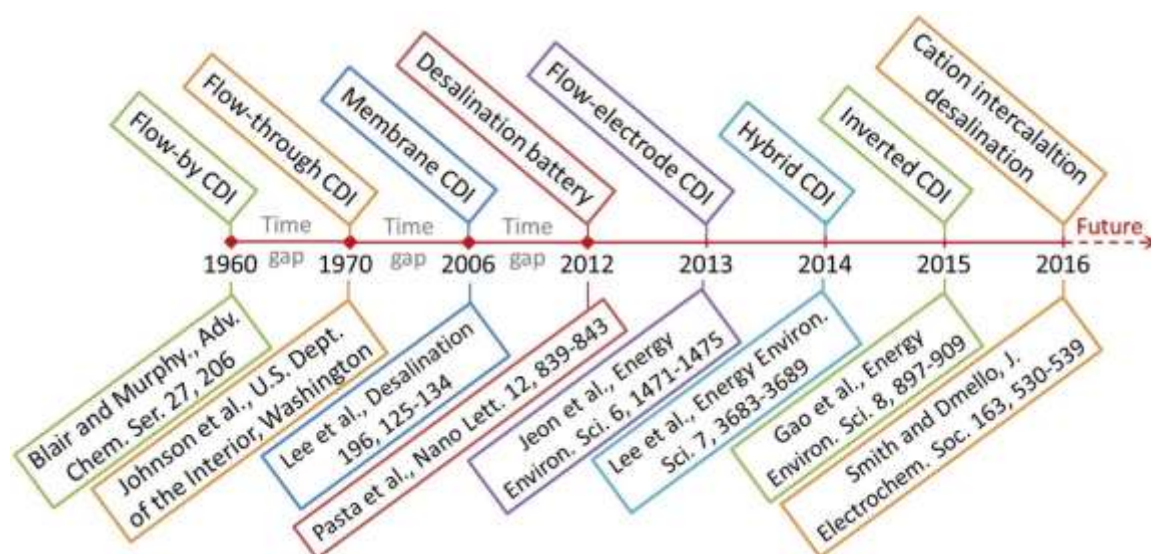
**Figure 2.2.    Timeline for the development of various cell architectures**

The Flow Electrode Capacitive Deionization (FE-CDI) cell was first developed in 2013 [16] as a modification of the MCDI style cell. It differed from all previously pioneered cell designs in the fact that stationary electrodes were replaced by two sets of particle suspension slurries that recirculated through the serpentine channels carved into the current collectors of the cell. This setup is schematically shown in Fig. 3.1. A conventional CDI system runs deionizing cycles until the stationary electrodes are saturated and have reached their maximum adsorption capacity. At the saturation point, the cell operation is halted and the applied potential is reversed (or removed) to allow electrode regeneration. Hence, during switching, conventional CDI runs the risk of cross-contamination between purified and concentrated streams, which overall reduces the purification efficiency. In addition, the mechanical switching of the cell potential curtails its effluent productivity. At a given time, the cell can either be purifying or concentrating. On the other hand, an FE-CDI system can run over several identical cycles as adsorption and regeneration can occur simultaneously. As shown in Fig. 2.3. [17], an applied operational CDI setup contains two identical cells that are oppositely biased. The electrode effluent from the cathode channel

of the first cell forms the influent into the anode channel of the second cell (and vice versa), hence allowing the suspension to recirculate continuously. The inclusion of ion exchange membranes prevent the cross mixing of the electrode streams with the inlet water streams. The two operating cells generate purified and concentrate streams concurrently with no risk of cross contamination. Hence increasing overall productivity of the system.
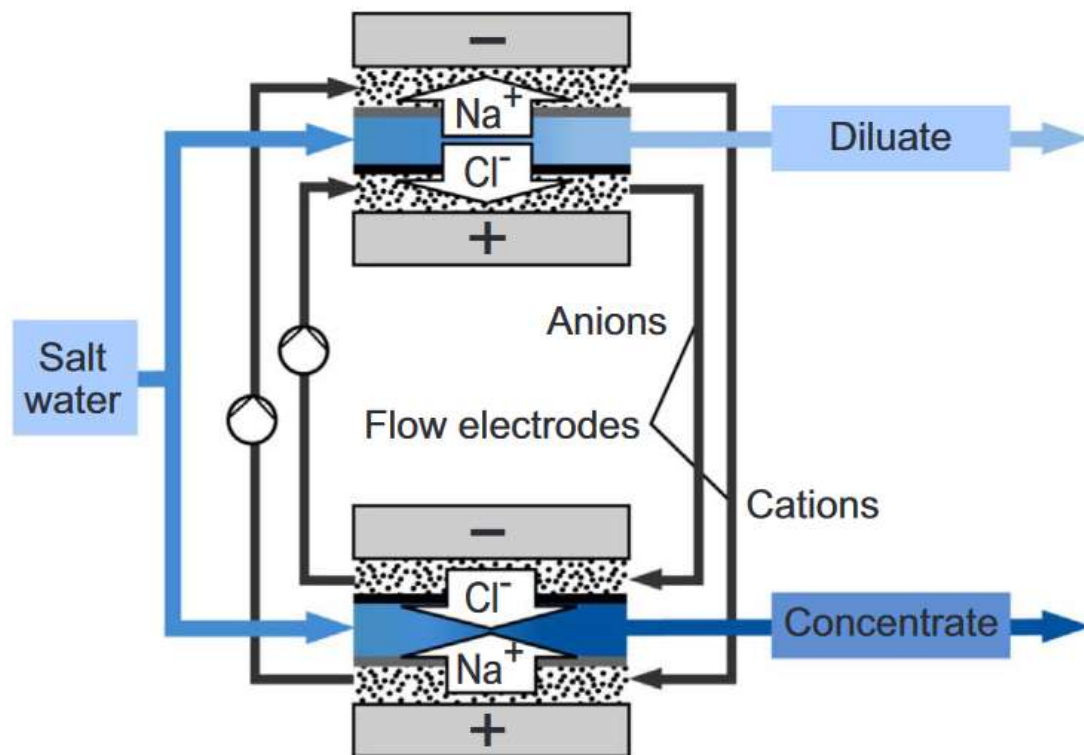


**Figure 2.3.     Two cell FE-CDI setup in continuous operation [17].**

CDI cell performance is evaluated by analyzing the changing ion concentration as a function of time. Several monovalent salt solutions, including NaCl, KCl, and NH$_4$Cl, exhibit a linear relationship between solution conductivity and ionic concentration. For this reason, effluent solution conductivity can be used as a stand-in for the changing ionic concentration. The later can be measured through a single-pass (SP) experiment or batch-mode (BM) experiment as shown in Fig. 2.4. [18]. As is apparent by the name, in an SP

experiment, the wastewater is passed through the cell only once and the effluent conductivity is measured at the outlet. It reaches a minimum and steadily rises again as electrodes are saturated and no more adsorption occurs (Fig. 2.4.a). In a BM experiment, the wastewater is circulated through the CDI cell until a low-minimum is reached and maximum ions have been adsorbed. In an FE-CDI cell, the electrodes are never completely saturated because the adsorption-desorption occurs simultaneously. Hence, SP style is infeasible and for this project, BM style experimental setup was used (Fig. 3.1. a).
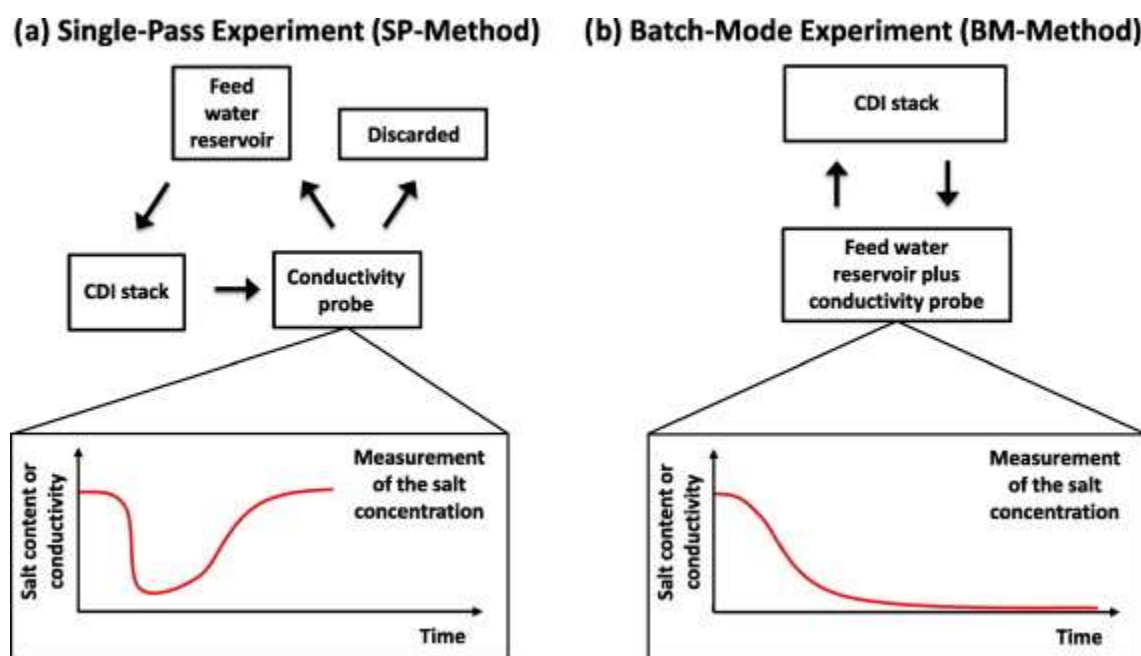


**Figure 2.4.    Schematic of two common experimental designs for CDI [18].**

A CDI cell is meant to be operated continuously. Hence performance metrics are evaluated once dynamic equilibrium (DE) has been reached. In DE, each charge-discharge cycle is identical to the last one. This is similar to the cyclic operation of batteries, and supercapacitors. Ideally, once DE has been achieved, the system should be able to operate continuously *ad infinitum*.

While CDI debuted as a desalination technology, its application are far-reaching and widespread (Fig. 2.5. [19]). This project demonstrates that CDI is a novel, adaptable, and versatile technology that can be used for applications beyond the facile treatment of brackish water. This also demonstrates that there is significant room for further research and development in the area.



**Figure 2.5.    Different applications of CDI technology [19].**

## 2.2.    Electrochemical Energy Storage

The technology of CDI draws inspiration from electrochemical capacitors that are also referred to as electric double-layer capacitors (EDLC) due to their primary charge storage mechanism. Charges in electrical devices (batteries, conventional capacitors etc.) are accumulated by either one or a combination of the mechanisms outlined in Fig. 2.6. [20]. EDLC storage (Fig. 2.6.a) exploits the directional electrostatic interactions that develop at the electrolyte/electrode interface. The polarized ions aggregate at the charged electrode/electrolyte boundary. Opposite ions in the electrolyte solution migrate towards the first layer aggregated ions to maintain charge neutrality. The concentration of the held charges decreases exponentially with increasing distance from the surface, as described by the Gouy-Chapman theory [21]. The mechanism of electrical double layer adsorption is facilitated by lattice morphology, as well as the nature of the electrolyte [22]. Hence, it is observed that EDL interfaces are highly prevalent in systems and materials that have a large surface area to volume ratio [22]. Therefore, charge accumulation via EDL storage can be characterized as a surface phenomenon.
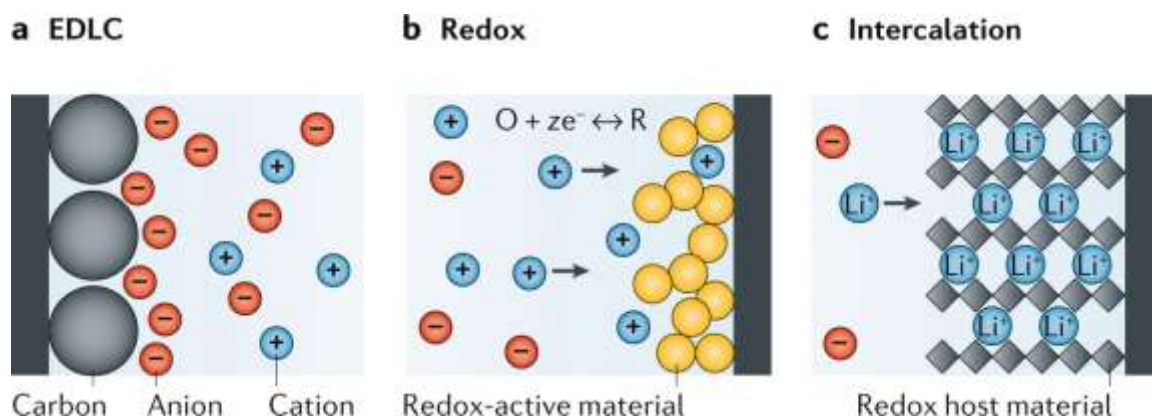


**Figure 2.6.    Three classes of charge storage mechanisms [20].**

The charge storage capacity can be enhanced via Faradaic or redox reactions. Functional groups on the charge storage material surfaces facilitate usable electrochemical activity. Electron charge transfer between the solvated electrolyte ions and the electrode surface (or ions in case of aqueous media) induces the formation of dynamic double layers within the electrolyte or at the interface surface. The charge transfer is rapid and vigorous. Ideally, no chemical bonding or reaction takes place. Faradaic charge storage (referred as pseudocapacitance) occurs in conjunction with EDL storage and is affected by the surface groups on the electrode materials and the affinity of solvated ions to the electrode material. In addition, in an aqueous media, Faradaic reactions can induce hydroxide ($OH^-$) ions which can increase total capacitance via hydrogen bonding storage.

The intercalation charge storage varies from the other two mechanisms that it utilizes the bulk of the electrode material instead of just the surface. It refers to the reversible insertion of a molecule or solvated ion into the interlayer spacing in layered materials. Development of intercalation based charge storage devices is still in the research and development (R&D) phase. Research efforts are concentrated towards the development and employment of a layered crystal structure material that offers rapid two-dimensional (2D) ion transport pathways.

Intercalation of ions in layers of a surface sensitive, redox-active material can allow for all three charge storage mechanisms to be in play simultaneously. Hence leading to charge storage systems that promise high power density, energy density, and long cyclability.

## 2.3.    MXenes

Ever since the isolation of graphene in 2004 [10], the world of layered and 2D materials has grown exponentially. This increased interest is fueled by the distinctive combination of thermal, optical, electrical, and magnetic properties brought out by the unique morphology of the lateral size being several times larger than the material thickness [23]. Since then many different 2D materials including hexagonal boron nitride (hBN), $MoS_2$, borophene, black phosphorous, silicone, and transition metal dichalcogenides (TMDs) have been discovered and extensively researched [23].  MXenes were first discovered in 2011 and are a novel class of 2D transition metal carbides, nitrides, or carbonitrides that exhibit a combination of unusual properties like high metallic conductivity, high surface area layered morphology, and hydrophilicity [24]. They have the general formula $M_{n+1}X_nT_x$ where M is an early transition metal, X is either carbon, nitrogen, or both while $T_x$ represents the surface termination group [25]. As shown in Fig. 2.7. [25], various different combinations of MXenes are possible, allowing for material development tailored for specific applications. MXenes are characterized by their layered atomic structures. Each layer has a sandwich-like structure, where each transition metal (M) atom bonds with C or N (or both) atoms in the central layer of atoms.

$Ti_3C_2T_x$ was the first MXene to be discovered and was our material of choice for this project [25]. Experimental and theoretical investigation of $Ti_3C_2T_x$ have uncovered several desirable properties that align with desired properties needed in CDI electrode materials. These include ecological safety, hydrophilicity, high electrical conductivity, colloidal stability, high capacitance, and scalability. In addition, the use of $Ti_3C_2T_x$ in capacitors is well documented and they exhibit volumetric capacitance as high as 786 F/g

[26]. This allowed us to hypothesize that $Ti_3C_2T_x$ would be a high performing material for FE-CDI.

MXenes are synthesized by selectively etching the A-layer (corresponding to an A group element) form the precursor MAX phases. The MAX phases belong to space group $P6_3/mmc$ and are comprised of a layered hexagonal structure. The A element layers are inserted in between the closely packed M-layers which have octahedral sites occupied by the X element atoms. In other comparable layered materials such as TMD's, weak van der Waals interactions are primarily responsible for holding the layers together. However, in MXenes, the M-X bonds is covalent/ionic (material dependent) in nature, while the M-A bond is metallic. If for a particular MAX phase, the M-A bond is weaker than the M-X bond, the phenomenon of relative bond energies can be used to selectively etch the A element by the use of strong acids or molten salts without disrupting the M-X bonds. It is important to note that the M-X bond strength is not greater than the M-A bond strength in all MAX phases and hence those MAX phases cannot be converted to MXenes. MAX phases with equivalent M-A and M-X bond strengths (e.g. $Cr_2AlC$) also do not respond to acid etching. However, in $Ti_3AlC_2$, the M-A bond is indeed weaker (0.98 eV) than the M-X bond (1.21 eV) , allowing it to be successfully exfoliated via acid etching [27].

In 2011, Naguib et al. [28] etched $Ti_3AlC_2$ using hydrofluoric acid to form $Ti_3C_2$ MXenes. The method has since been modified to what is currently known as the minimally intensive layer delaminated (MILD) method which produces in-situ HF. Shown in Fig. 2.8. [29] the MILD method is the most prevalent synthesis route because of it eliminates the need for a separate delamination step, is relatively safer, and has been shown to be scalable without loss of properties [30].
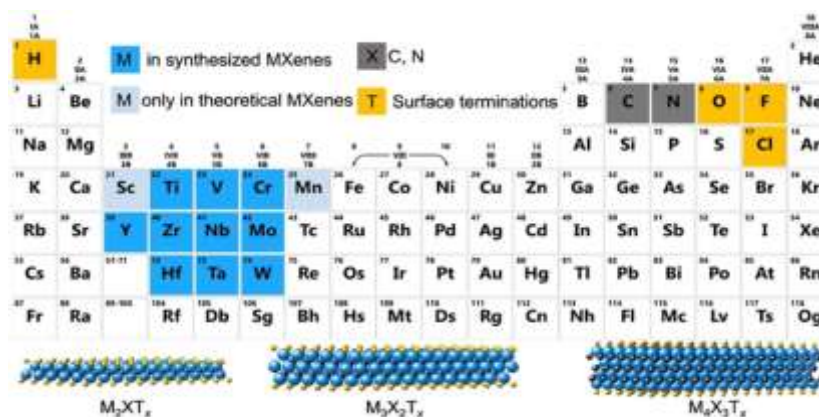
**Figure 2.7.    Periodic table showing various combinations of MXenes [25].**

Some studies have shown successful etching using alternate routes [31] but the process suffers from extremely low yield and is not viable. Reaction parameters such as the size of MAX phase powder, etching time, temperature, and HF concentration can vary the yields, etching times and quality of the produced MXenes. As shown in Fig. 2.8. [29], the non-single step clay method yields multi-layer (ML) MXenes while the prevalent MILD method gives few-layer (FL) MXenes. The end application must be in sight when selecting the suitable synthesis route. For this application as CDI electrode, MILD method was selected because of few layer MXenes have higher surface area which is desirable in this case.
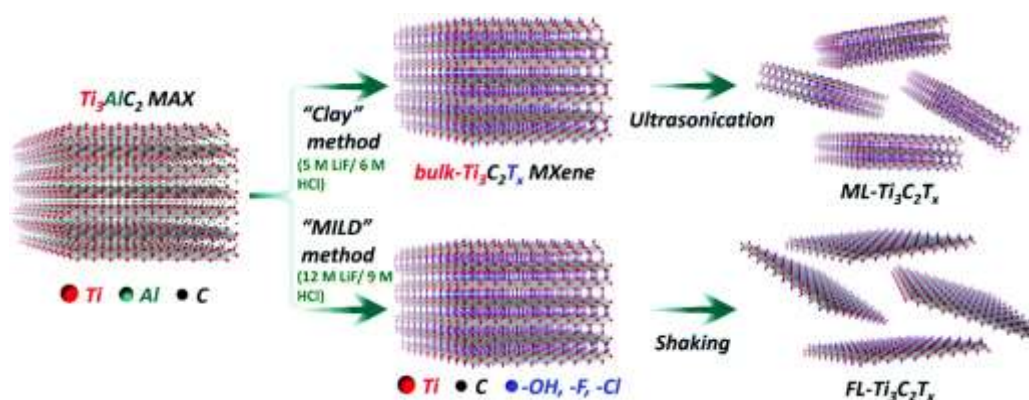


**Figure 2.8.    Etching routes for $Ti_3C_2T_x$ MXenes [29].**

The MILD method for selective etching follows the given steps:

I. 1.6 g of LiF salt is added to previously measured 20 mL of HCl in a polytetrafluoroethylene (PTFE) container housing a Teflon coated magnetic stir bar. The mixture is stirred for 2-3 minutes at 200 rpm until the salt has visibly dissolved.

II. 1 g of $Ti_3AlC_2$ is added to the salt mixture in five increments over the course of ten minutes.

III. The reaction is allowed to run at 300 rpm for 24 hrs at room temperature and pressure.

IV. The mixture is carefully poured into a centrifuge tube and 30 mL of deionized (DI) water is added to it.

V. The solution is centrifuged at 3500 rpm for 5 minutes.

VI. Following the centrifugation, the MXenes "clay" would have settled at the bottom. The supernatant is decanted and its pH is measured. Then fresh DI water is added before resdispersing the clay.

VII. Step V and VI are repeated until the pH of the supernatant is neutral (~ 7) and the supernatant is black in color. The dark supernatant indicates that MXenes have delaminated.

VIII. The dark supernatant is decanted into a glass container. The unreacted MAX at the bottom of the centrifuge tube is discarded.

IX. The supernatant solution can be vacuum filtered and vacuum dried to obtain MXene powder.

Delaminated MXenes form a stable colloidal solution and no surfactants are necessary. Spontaneous delamination occurs during the MILD etching process because the Li+ ions intercalate between the layers along with hydration shells of $H_2O$. The two weaken the bonding between the flakes and hence facilitate the delamination process.

The size of the obtained MXene flakes can be controlled via adjusting the speed and time during centrifugation. However, it is more convenient to do a particle size analysis following synthesis and then alter the size distribution by probe sonicating under argon. Since MXenes are prone to oxidation, they are stored in a controlled environment like a glove box.

The etching of $Ti_3AlC_2$ is believed to proceed as follows [28]:

    I.    $Ti_3AlC_2 + 3HF = AlF_3 + 3/2H_2 + Ti_3C_2$

    II.    $Ti_3C_2 + 2H_2O = Ti_3C_2 (OH)_2 + H2$

    III.    $Ti_3C_2 + 2HF = Ti_3C_2F_2 + H_2$
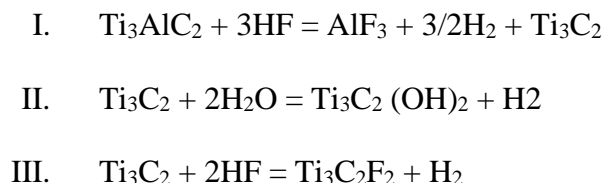
To confirm the successful synthesis of MXenes, XRD is the most common technique employed. The conversion of MAX phase to multilayer MXene changes the characteristic XRD pattern. $Ti_3AlC_2$ MAX phase shows all crystallographic peaks a expected from the $p6_3/mmc$ structure. Hydrated $Ti_3C_2T_x$ (delaminated with water intercalated, as mentioned earlier) exhibit highly broadened (00$l$) peaks. It is also common that higher ordered peaks representative of peaks representative of $a$ lattice reflections disappear. Delaminated MXene will give only (00$l$) peaks. The most characterstic is the (002) peak, as it is indicative of the $c$-lattice parameter. Due to the layered nature, the interlayer spacing will readily change to accommodate intercalants. Hence the location of the (002) peak can inform about the thickness of

the MXene sheet. If intercalation is of interest, the change in interlayer spacing can help

determine the storage mechanism and the amount of ions stored in between the

layers. Typically, XRD is done to confirm the successful synthesis of MXenes, by

observing the (00$l$) peaks. The following equation derived from Bragg's Law is used to

determine interlayer spacing in MXenes [32]:

$$\frac{1}{d^2} = \frac{4}{3}\left(\frac{h^2 + hk + k^2}{a^2}\right) + \frac{l^2}{c^2}$$

The etching can also be confirmed by observing the obtained samples under

Scanning Electron Microscope (SEM) and Transmission Electron Microscope (SEM).

The classic accordion like structure of etched can be observed in an SEM images as

pointed out by the arrows in Fig. 3.2.d. The exfoliation is evident when contrasting

against the SEM image of the $Ti_3AlC_2$ MAX phase (Fig. 3.2.d. inset). The TEM

micrographs (Fig. 3.2.c), confirm that the $Ti_3C_2T_x$ stacks are formed of electronically

transparent few layers (as marked by the arrows).

### 2.4.    Hypothesis

Due to the colloidal stability, higher number of surface sites, and layered structure

that facilitates intercalation, we hypothesized that $Ti_3C_2T_x$ Mxene solution would *achieve*

*higher adsorption capacity* compared to prevalent carbon electrode materials in flow

electrode CDI systems. Our hypothesis was supported by the high affinity of $NH_3$ gas on

$Ti_3C_2T_x$ Mxene as shown in gas sensor studies [33]. In addition, $Ti_3C_2T_x$ Mxenes had

shown excellent ion storage capacity in pseudocapacitor application studies [34].

CHAPTER THREE: MANUSCRIPT

### 3.1.Abstract

Flow electrode CDI systems (FE-CDI) have recently garnered attention because of their ability to prevent cross contamination, and operate in uninterrupted cycles ad infinitum. Typically, FE-CDI electrodes suffer from low conductivity, which reduces deionization performance. Higher mass loading to combat low conductivity leads to poor rheological properties, which prevent the process from being continuous and scalable. Herein, $Ti_3C_2T_x$ MXenes were introduced as 1 mg/mL slurry electrodes in an FE-CDI system for the removal and recovery of ammonia from stimulated wastewater. The electrode performance was evaluated by operating the FE-CDI system with a feed solution of 500 mg/L $NH_4Cl$ running in batch mode at a constant voltage of 1.2 and -1.2 V in charging and discharging modes respectively. Despite low loading compared to activated carbon solution, $Ti_3C_2T_x$ flowing electrodes showed markedly improved performance by achieving 60% ion removal efficiency in a saturation time of 115 minutes, and an unprecedented adsorption capacity of 460 mg/g. The system proved to be a green technology by exhibiting satisfactory charge efficiency of 58-70% while operating at a relatively low energy consumption of 0.45 kWh/kg when compared to the current industry standard nitrification-denitrification ammonia stripping process. A 92% regeneration efficiency showed that the electrodes were stable and suitable for long term and scalable usage. The results demonstrate that MXenes hold great potential in improving the FE-CDI process for energy-efficient removal and recovery of ammonium ions from wastewater.

## 3.2.    Introduction

Energy and water exist in a complex symbiotic relationship; energy production has a water footprint, while water remediation and supply efforts exert a strain on the power resources. Nuclear and coal power plants require between 20 to 60 gallons of freshwater for every kilowatt-hour (kWh) of energy generated [35]. Correspondingly, water remediation and recovery efforts consume 2% of the total energy generated in the United States [36], [37]. Environmental efficiency and economics encourage conservation of both resources. Water itself is an abundant resource but only 2.5% is readily accessible as freshwater, and there are already countries that rely on remediation efforts to obtain their water supply [38]. As the global population continues to rise, energy and water consumption will increase while existing natural sources will continue to be depleted. In its annual 2019 report, the International Energy Agency (IEA) predicts an 85% increase in energy related water usage in the upcoming years [37]. In light of this projection [37], it is imperative that versatile, cost-effective, and energy-efficient water technologies are developed. Wastewater reclamation is one step in a multi-stage solution to solve the looming freshwater availability crisis. Wastewater reclamation is environmentally as well as fiscally relevant because it can yield purified effluent, as well as recover embedded resources.

Ammonia is one of the most common contaminants found in domestic and industrial wastewaters. Yet, due to its importance in the agricultural industry, ammonia is one of the most industrially produced chemicals, with over 14 million metric tons produced in the United States alone in 2019 [39], [40]. The production of ammonia requires copious amounts of both energy and water. While ammonia is undeniably a valuable building block

in the modern food production, excessive exposure is a valid concern, due to its toxicity [39], [41]. The release of ammonia rich wastewater to into aquatic ecosystems can cause eutrophication, leading to disruptions in delicate ecological balances [42]. Owing to these detrimental effects, the Clean Water Act (CWA) prohibits industrial facilities from releasing nitrogen (as ammonia) rich wastewater to waterbodies [8]. Considerable effort has been devoted to developing efficient ammonia removal methodologies [43]. Despite that, biological nitrification remains the most widespread method for treating ammonia wastewater [44]. Aside from being cumbersome and slow, it also wastes embedded ammonia, which is otherwise a valuable product. In pursuit of sustainability, product conservation directly translates to energy conservation. Hence, there remains room for a technology that is energy, water, and resource efficient.

Prevalent water remediation technologies such as reverse osmosis, multiple effect distillation, and multistage flash distillation require anywhere from 2-58 $kWh/m^3$ of direct energy input [45]. Reverse Osmosis (RO) is the most common technique, and typically uses 2-10 $kWh/m^3$ of power [46]. Among purification technologies, capacitive deionization (CDI) has been a promising contender. It is an electrophoretic technique that uses a small voltage (~ 1.2 V) applied across two high surface area electrodes to induce charge separation. Similar to a supercapacitor, the charges are stored in the electric double layer of the electrodes. Even though there has been increasing research interest in CDI [47], the unavailability of adequate electrode materials acts as a bottleneck for the technology. Since voltage reversal (or removal), causes desorption of the immobilized ions, the technique can be used for purification as well as retrieval. Several studies report high water recovery (80-90%) and low energy utilization (0.6 $kWh/m^3$) for desalination using CDI [48]–[50].

As a result of an increased research activity around CDI [47], several different cell architectures have been developed including inverted-, hybrid-, ultrafiltration-, flow-by-, desalination battery, membrane-, flow-through-, cation intercalation desalination, and flow-electrode CDI (FE-CDI) [15]. Apart from FE-CDI, all of these cell architectures utilize stationary electrodes and hence require an additional regeneration step for ion desorption, leading to non-continuous operation [15], [51]. Additionally, the regeneration step can cause cross-contamination between the effluent streams, resulting in lower water recovery [52]. This step negatively affects the fundamental motivators for CDI technology: cost, time, and energy efficiency. Due to the ability to regenerate electrodes simultaneously, FE-CDI is a pioneering electrochemical technology that promises continuous, infinite remediation even for high concentration feed waters [53]. The adsorption capacity of the system is controlled by regulating the flow rate, channel design, and the nature and loading of the electrode material.

Carbon and its derivatives such as graphene sponge, graphene oxide, carbon nanotubes (CNTs), and various composites have been investigated as CDI electrodes [54]. Carbon serves as an excellent prototype material due to its high surface area, electrical conductivity, and electrochemical stability [54]. While carbon materials have been shown to perform well in stationary electrode cell architectures [55], they suffer from low electrical conductivity in a slurry electrode systems [56]. In prior studies, and in our experimental experience, remediating the conductivity problem by increasing carbon content ($> 15$ wt.%) leads to clogged flow channels, halting operation.

MXenes are a class of two-dimensional (2D) transition metal carbides, nitrides and carbonitrides with the general formula $M_{n+1}X_nT_x$ where M is an early transition metal (Ti,

V, Nb, etc.), X is carbon and/or nitrogen, $T_x$ represents the surface terminations (=O, -F, -Cl, and -OH), and n = 1-4 [57]. The family of materials is highly conductive, hydrophilic, and can be scalably produced with no loss of properties [30], [58]. MXenes have already been proposed as materials useful for environmental remediation, including heavy metal adsorption, pollutant adsorption, desalination, amongst others [59], [60]. $Ti_3C_2T_x$ was the first MXene discovered and is the most widely studied [28]. Furthermore, $Ti_3C_2T_x$ was shown to pose no ecological risk to aquatic ecosystems [61]. Recently this material has been applied to conventional CDI owing to high surface area and electrical properties [62]–[66].

Many studies have shown that $Ti_3C_2T_x$ is a promising pseudocapactive anode for supercapacitors [24], [67]–[69]. Ideal materials for aqueous electrochemical energy storage should have high specific capacitance, charge efficiency, and electrochemical stability at water electrolysis potential (~ 1.23V) [70], [71]. These features are also required in high performance CDI electrodes, suggesting that $Ti_3C_2T_x$ will be appropriate for CDI systems. Wang et al. demonstrated the use of aerogel-like $Ti_3C_2T_x$ MXene electrodes in a conventional desalination CDI cell to report an unprecedented salt adsorption capacity of 45 mg/g [72]. In a recent publication, Ma et al. used binder free pristine $Ti_3C_2T_x$ films to achieve a salt adsorption capacity of 68 mg/g [62]. However, conventional CDI cells invariably experience co-ion expulsion, which reduces their charge efficiency [73]. The necessity of a regeneration step in conventional CDI invariably increases energy consumption [51], [52]. For CDI to be considered a green technology, it is necessary to account for the operating energy. The use of ion exchange membranes in the cell reduces co-ion expulsion. High charge efficiency leads to low operating energy. With energy,

water, and resource conservation, FE-CDI holds the promise to surpass the limitations of the preceding water remediation technologies including the widespread RO systems.

In the present study, we aim to evaluate the de-ammonification performance of $Ti_3C_2T_x$ flow electrodes in an FE-CDI system. This has been schematically shown in Fig. 3.1. This work demonstrates the suitability of $Ti_3C_2T_x$ MXenes as high performance, low loading flow electrodes. It also opens avenues for further exploration in using other MXenes in CDI technology.
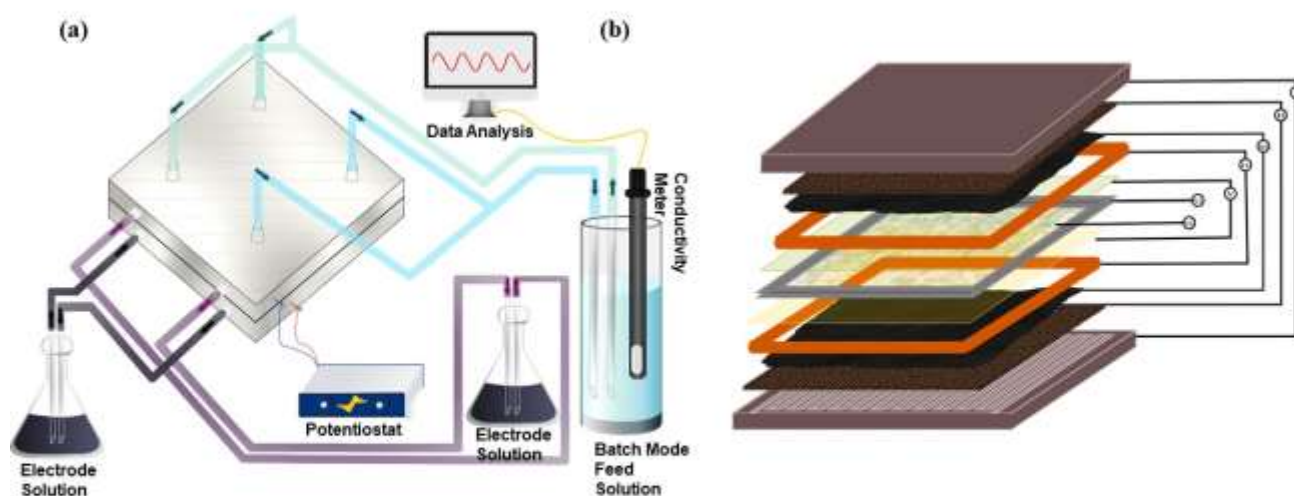


**Figure 3.1.     Schematic illustration for (a) FE-CDI module for deionization testing, and (b) CDI unit cell assembled with: i) Titanium Current Collectors ii) Vitreous Carbon iii) Carbon Cloth  iv) Rubber Gaskets v) Anion and Cation Exchange Membranes vi) Spacer vii) Polyester Filter Felt.**

## 3.3    Experimental

### 3.3.1. Preparation of Activated Carbon Flow Electrodes

The 10 wt.% control flow electrodes were prepared by mixing 1.2 g of 80 mesh activated carbon (AC) powder (Cabot Norit® A Ultra E 153) in 12 mL of nanopure water and stirring for 2 hours. The mixture was probe sonicated for 1 hour at 55 W to reduce the particle size by breaking up agglomerates, increasing the flowability. During cell operation, the electrodes were continuously stirred using a magnetic stir bar to prevent sedimentation of the carbon particles.

### 3.3.2. Preparation of $Ti_3C_2T_x$ Flow Electrodes

$Ti_3C_2T_x$ MXenes were etched from commercially obtained $Ti_3AlC_2$ MAX Phase (2D Semi-Conductors) using the minimally intensive layer delamination (MILD) synthesis method 38]. This method was selected because of its reduced toxicity, and the ability to produce low defect, larger MXene flakes [74], [75]. 20 mL of 9 M hydrochloric acid (HCl, Alfa Aesar) was stirred with 1.6 g of Lithium Fluoride (LiF, 99.85% Alfa Aesar) using a Teflon magnetic bar at 300 rpm for 10 minutes prior to addition of the MAX. 1 g of $Ti_3AlC_2$ was added to the *in-situ* synthesized HF solution in four increments to prevent overheating of the solution. The reaction was allowed to run for 24 hours at room temperature and ambient pressure (RTP). The resultant mixture was then washed using nanopure water via centrifugation at 3500 rpm until the acidic supernatant became neutral (pH 5-6). The presence of lithium ions ($Li^+$) with the etching solution causes simultaneous etching/delamination resulting in an electrostatically stable colloidal solution. The stable supernatant was vacuum filtered with a glass microfiber filter (0.45 µm, Whatman) to separate the MXene clay. To prepare the flow electrode solution, the MXene residue was

re-dispersed in nanopure water via manual shaking to obtain a solution with concentration of 1 mg/mL (0.1 wt.%).

### 3.3.3. Characterization of $Ti_3C_2T_x$

To evaluate the morphology and structure of the samples, several characterization techniques were employed. X-ray diffraction (XRD) was conducted on a Rigaku Smartlab equipped with a Cu Kα source, a step size of $0.03°$, and a holding time of 0.5 s from 3-90°. The characteristic expanded structure of the MXenes was observed via scanning electron microscopy (SEM) and transmission electron microscopy (TEM) imaging on the FEI Teneo Field Emission SEM and JEOL JEM-2100 HR analytical TEM respectively. Microscopic imaging was also used to map out lateral size of the flakes, which was further confirmed by dynamic light scattering (DLS) performed on a Brookhaven NanoBrook Omni. The obtained measurement is the hydrodynamic diameter, where the particle is assumed to be spherical in nature. It is a function of diffusion co-efficient according to the Stokes-Einstein relation. The measurement is an effective average, and hence can deviate from actual lateral flake size. The tool was also used to measure electrophoretic mobility of the colloidal suspension. All measurements were taken at RTP (25 °C, 1 atm) and at 7 pH. The viscosity of the colloidal suspension was measured on a RheoSense µVisc Viscometer with 300 µL of solution to obtain five repeated measurements. Raman spectra was obtained using a 532 nm He−Cd laser on a Horiba LabRAM HR Evolution Raman by drop casting the electrode solution on a glass slide.

### 3.3.4. Capacitive Deionization Experiments

To evaluate the performance of the electrodes, a self-assembled CDI unit with titanium current collectors of dimensions 6.35 cm x 6.35, carved with serpentine flow

channels, was operated in batch mode in constant voltage (1.2 V) cycle in both charging and discharging stages. The power was sourced from a Biologic SP-50 potentiostat. The effective contact area was 10 cm$^2$. As shown in Fig. 3.1.a, the cell was assembled with vitreous carbon (Duocel Reticulated Vitreous Carbon 100 ppi), carbon cloth (AvCarb 1071 HCB), rubber gaskets (Neoprene, 1.5 mm), along with pre-treated anion and cation exchange membranes (Fumasep FAA-3-PK-130 and Nafion™ 115 respectively). These were separated by a non-conductive porous spacer (Nylon 3/64") with a polyester filter felt (50 μm) that allowed the feed water to pass through. 20 mL of 0.5 mg/L ammonium chloride (NH$_4$Cl) solution was prepared by dissolving analytical grade NH$_4$Cl (99.99% Sigma Aldrich) in deionized water (18 MΩ-cm). The solution was circulated through the cell at a flow rate of 2 mL/min while a conductivity meter (HACH H1440d Benchtop Meter) monitored the conductivity of the NH$_4$Cl solution. 6 mL each of the two electrode solutions were circulated in the cell channels at a flow rate of 3 mL/min.

3.3.5. Performance Metrics

To evaluate the performance of Ti$_3$C$_2$T$_x$ MXene (and AC) electrodes in the FE-CDI cell, the following equations were used to calculate the given metrics [76]:

I.   Conductivity ratio, $Cf/C_o = \dfrac{C_o - C_f}{C_o}$

II.  Deionization efficiency $= \dfrac{C_o - C_f}{C_o} \times 100\ \%$

III. Deionization capacity, $\Gamma = \dfrac{(C_o - C_f)(Vol)}{m}\ mg/g$

IV.  Adsorption rate $= \dfrac{(C_o - C_f)(Vol)}{At_{adsorb}}\ mg/min/cm^2$

V.   Charge Efficiency, $\Lambda = \dfrac{(F)(\Delta M)}{Q_{in}}\ \%$

VI.  Coulombic efficiency loss, $\eta_{coul} = \dfrac{Q_{out}}{Q_{in}} \times 100\%$

VII.    Electrode regeneration efficiency, $\eta_r = \dfrac{\Gamma_n}{\Gamma_i} \times 100\%$

VIII.    Energy Consumption $= \dfrac{(V)(Q_{in})}{3600(C_o - C_f)_{adsorb}(Vol)}\ kWh/kg$

IX.    Energy Recovery $= \dfrac{\dfrac{(V)(Q_{out})}{3600(C_o - C_f)_{desorb}(Vol)}}{Energy\ Consumption} \times 100\%$

Where,

$C_o$ = Initial concentration of effluent solution (mg/L)

$C_f$ = Final concentration of effluent solution (mg/L)

Vol = Volume of feed solution (L)

m = Mass of particle loading in electrode slurry (g)

A = Contact area between electrode flow channel and ion-exchange membranes (cm$^2$)

t = Time of adsorption cycle (min)

$\Delta M$ = Moles of NH$_4$Cl removed (mol)

F = Faraday's constant (96485 C/mol)

$Q_{in}$ = Charge uptake during adsorption (C)

$Q_{out}$ = Charge release during desorption (C)

$\Gamma_n$ = Deionization capacity of the final cycle (mg/g)

$\Gamma_i$ = Deionization capacity of the initial cycle (mg/g)

V = Voltage applied across the cell (V)

## 3.4.    Results and Discussion

3.4.1 Material Characterization
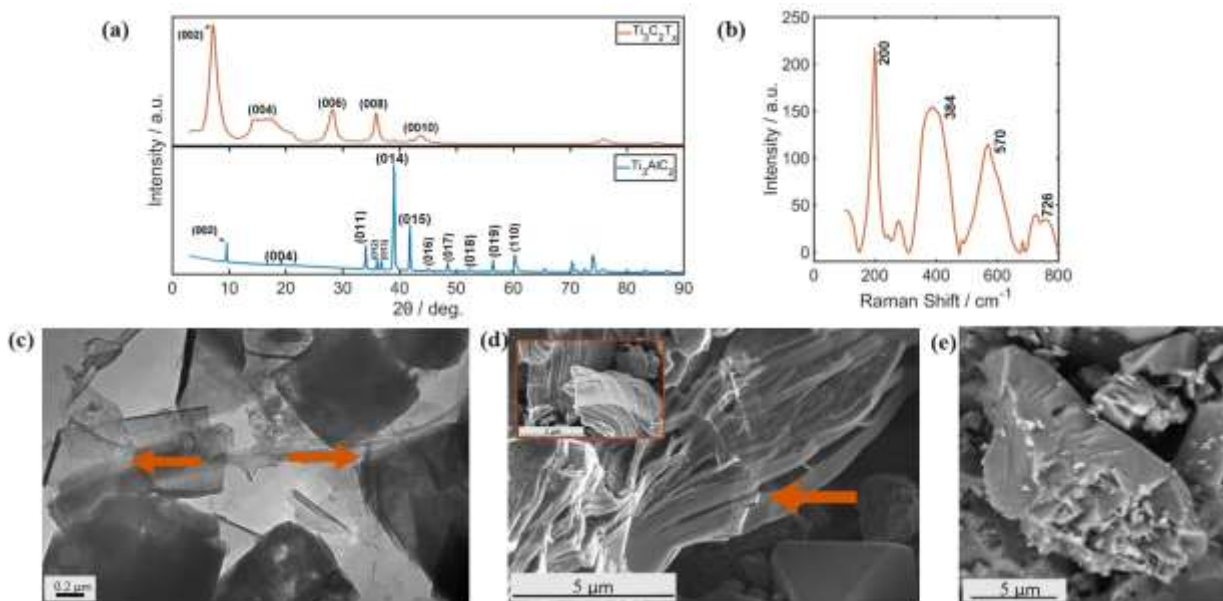


**Figure 3.2.    (a) XRD spectra of Ti₃AlC₂/ Ti₃C₂Tₓ before and after etching; (b) Raman spectra of Ti₃C₂Tₓ flow electrodes at 532 nm; (c) TEM image of etched and delaminated Ti₃C₂Tₓ showing separated layers.; (d) SEM image of etched and delaminated Ti₃C₂Tₓ (inset) SEM image of Ti₃AlC₂; (e) SEM image of AC powder particle**

XRD results shown in Fig. 3.2.a confirms successful etching of Aluminum (Al) from the $Ti_3AlC_2$ MAX phase by the shift in the (002) peak from 9.60° to 7.17°. In the MILD method, etching and delamination simultaneously, with delamination occurring through intercalation of water ($H_2O$), and lithium ions ($Li^+$). The ion removal mechanism in FE-CDI is dependent on the type of electrode material used [47]. Carbon electrodes operate through ion adsorption on the charged surface of the particles, while MXenes function by allowing ion insertion between the individual sheets [77]. Hence, the interlayer spacing has a pronounced effect on the charge storage and the ionic transport properties of MXenes [78]. The etched $Ti_3C_2T_x$ has a total interlayer spacing of 4.40 Å, due to the

intercalated water and lithium ions coupled with successful etching. The interlayer spacing determines if charge storage can occur via interaction. The ammonium ion has a diameter of 3.50 Å, hence making it viable for it to intercalate. This results in the characteristic expanded structure of MXenes, as shown in Fig. 3.2.d.

The Raman spectra in Fig. 3.2.b shows four distinct characteristic peaks at 200, 384, 570, and 726 cm$^{-1}$. The $A_{1g}$ peak at 200 cm$^{-1}$ and the $E_g$ peak at 384 cm$^{-1}$ correspond to vibrations due to surface groups on titanium. [79]. While the $E_g$ and $A_{1g}$ peaks observed at 570 cm$^{-1}$ and 726 cm$^{-1}$ respectively, can be attributed to carbon variations. [79]. The absence of sharp $E_{g1}$ peak (at 144 cm$^{-1}$) and positive shifting of the spectra can be attributed to the nanosized structure of the flakes [28], [79]. Line broadening and merging in the spectra is indicative of exfoliation and delamination and is hence consistent with the XRD data.

TEM image in Fig. 3.2.c shows stacked multilayer MXene sheets that are thin and electron transparent. The morphology and surface structure of the electrode particle materials have a significant effect on the ion adsorption capacity. The highly accessible surface, characterized by the expanded and open interlayer structure, allow for rapid ion adsorption within the MXene sheets [34]. The porous structure of AC is clearly observed in Fig. 3.2.e. The figure also exhibits the irregular block morphology of AC, with particle size ranging in a few microns. This is consistent with DLS particle size analysis (Fig. 3.3.a). The characteristic fanned out basal planes of etched MXenes can be seen in Fig. 3.2.d. It can be witnessed visually that the spread out, open structure of MXenes has significantly more intercalating space than the porous structure of AC. Moreover, the unfurled

morphology is evidence for successful etching of $Ti_3AlC_2$ (Fig. 3.2.d-inset) and is hence in

agreement with the aforementioned XRD and Raman results.

3.4.2. Flow Electrode Slurry Characterization
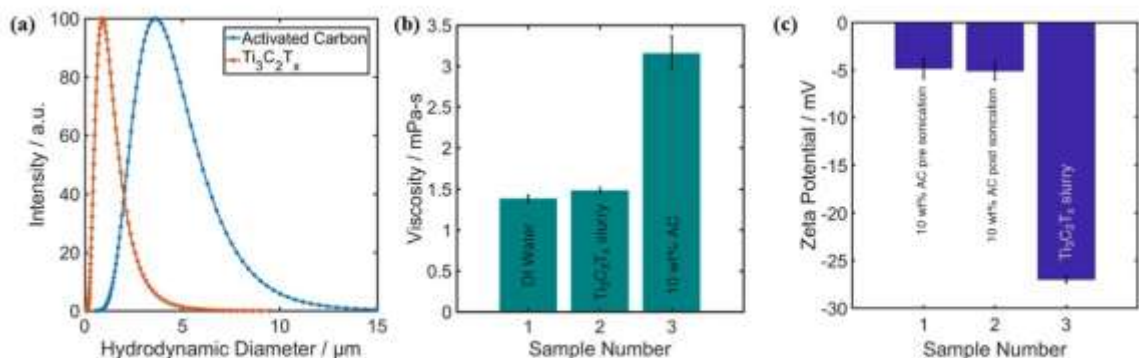


**Figure 3.3.** **(a) Particle size analysis of 10 wt% AC slurry electrodes and Ti3C2Tx flow electrodes; (b) Viscosity measurements of 1. DI Water, 2. $Ti_3C_2T_x$ flow electrodes, and 3. 10 wt% AC slurry electrodes; (c) Surface potential measurements of 1. 10 wt% AC slurry before sonication, 2. 10 wt% AC electrodes after sonication, and 3. $Ti_3C_2T_x$ flow electrodes.**

The flow electrode is the most important component of the FE-CDI cell. The

rheological properties and followability of the electrode contribute towards the

deionization capacity, stability, and cyclicality of the system. Due to homogeneity, stable

colloidal slurries perform better as flow electrodes. For colloidal suspensions, rheological

properties are a function of the size and concentration of the added dispersant [80]. Fig.

3.3.a shows particle size profiles of the 10 wt.% AC slurry and the $Ti_3C_2T_x$ electrodes. It is

evident that the average particle size is lower for MXene electrodes (1.2 μm) than AC (4.5

μm). In addition, the AC profile exhibits a wider distribution and longer tail end, indicating

particle flocculation. For this reason, the AC slurry was continuously stirred during the

experiment to prevent sedimentation. Furthermore, the viscosity of a suspension has a

strong correlation with particle size. Higher viscosity contributes to poor followability and

dispersion of the slurry. Fig. 3.3.b shows that the $Ti_3C_2T_x$ solution has a viscosity very close to deionized (DI) water (1.483 mPa-s and 1.382 mPa-s respectively). Experimentally, this resulted in excelled followability and zero hindrance during the cell operation. This can be attributed to the presence of hydrophilic functional groups on the surface of MXene layers which result in electrostatic repulsion that leads to a stable colloidal solution not prone to flocculation [58]. Comparatively, the third sample, AC slurry had a higher viscosity. Combined with larger particle size (Fig. 3.3.a); it led to poor followability and frequent clogging of the narrow cell channels in our conductor design. Zeta ($\zeta$) potential is an important guide to determine stability of suspensions. AC forms lyophobic colloids, which is reflected in its high (less negative) $\zeta$-potential value of -5 mV, as shown in Fig. 3.3.c. Sample 1 was prepared from as received 80 mesh AC powder, while sample 2 was probe sonicated for 1 hour to yield the particle size distribution given in Fig. 3.3.a. The two samples did not exhibit any considerable difference in $\zeta$-potential, as it is independent of particle size [80]. However, as aforementioned, reducing particle size had a positive impact on fluid flow. As apparent in Fig. 3.3.c, the $Ti_3C_2T_x$ solution had a considerably lower (more negative) $\zeta$-potential value of -27 mV, which resulted in electrode stability throughout the CDI operation.

3.4.3. Deionization Performance Test
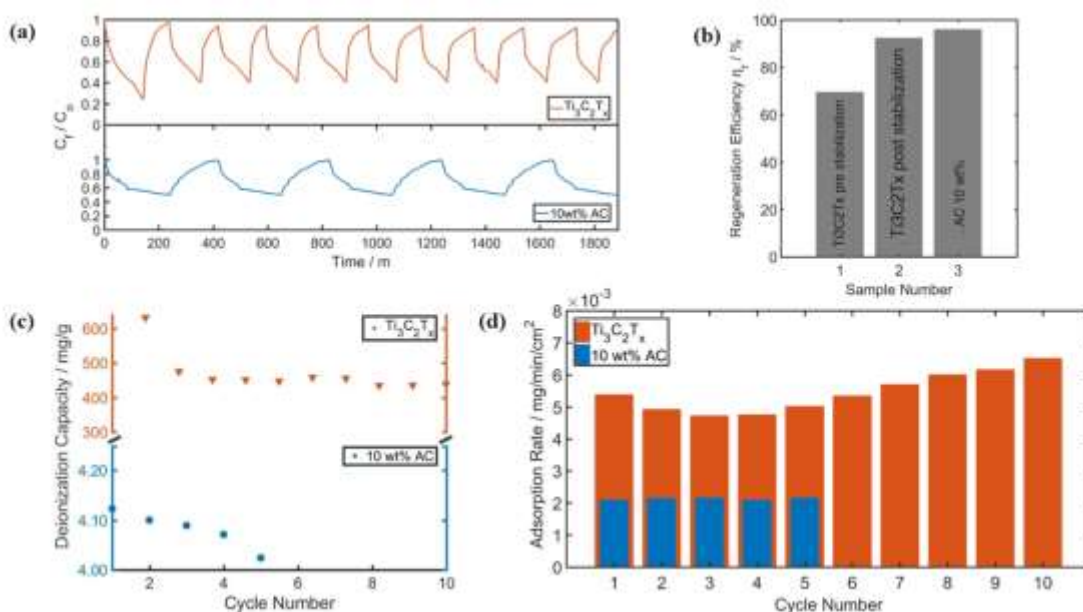


**Figure 3.4.     (a) Effluent conductivity showing electrosorption-desorption cycles; (b) Electrode regeneration efficiency of 1. Ti₃C₂Tₓ before stabilization 2. Ti₃C₂Tₓ after stabilization, and 3. AC; (c) Electrode adsorption capacity at each regenerative cycle; (d) Adsorption rate at each regenerative cycle.**

Fig. 3.4.a shows the change in conductivity ratio of the effluent solution as a function of time when the system was operated in batch mode. The observed cyclic conductivity change is representative of the ion capture and release steps during the regenerating operation. In this study, the 10 wt.% AC slurry was used as control electrodes to evaluate the performance of $Ti_3C_2T_x$. The conductivities of both deionization systems show a significant decrease with the application of 1.2 V external voltage. The open structure and intercalation capture mechanism in $Ti_3C_2T_x$ MXenes resulted in a shorter saturation time of 115 minutes compared to AC (233 minutes), and other previously reported studies [18], [81], [82]. Due to the shorter charge-discharge times, $Ti_3C_2T_x$ delivered 10 stable long-term cycles during the ~ 30 hour run time. This manifested in

twice the number of cycles as AC (5 cycles). As saturated electrosorption is achieved, the charging (ion capture) profile for $Ti_3C_2T_x$ plateaus at an average conductivity ratio of 0.4070, which is lower than the obtained value for AC (0.5008). It is interesting to note that the conductivity ratio of the first run in cycle with $Ti_3C_2T_x$ MXenes is markedly lower (0.2413) than the following cycles. In the first cycle, the system has not yet achieved dynamic equilibrium and the increased deionization is possibly a result of permanent chemical interactions on the defect sites on the MXene flakes [83]. These ions are not desorbed upon voltage reversal (or removal). Hence, the first cycle is not representative of the electrode performance. This is reflected in Fig. 3.4.b which shows electrode regeneration efficiency ($\eta_r$). After achieving dynamic equilibrium (sample 2), $\eta_r$ is upwards of 92%. If we take the first cycle into account, $\eta_r$ drops to 69.5% which is evident of the suggestion that after the initial cycle, some adsorption sites are permanently occupied by chemical interactions. It is imperative to note that $\eta_r$ for AC is slightly higher at 96%. This can be attributed to the oxidative and aqueous degradation of $Ti_3C_2T_x$ MXenes over time [84]. However, researchers have been working to increase oxidative stability of MXenes [85]. In addition, the use of MXenes in non-aqueous solvents as flow electrodes can be explored in the future [86].

Deionization capacity is an integral criterion to evaluate the electrode performance in a FE-CDI cell. The average deionization capacities exhibit great disparity between the two electrode systems. The average removal capacity for $Ti_3C_2T_x$ is 460 mg/g, or more than 2 orders of magnitude higher than AC, with average removal capacity of 4.2 mg/g. The values for each charge-discharge cycle are shown in Fig. 3.4.c. It can clearly be seen that deionization capacity decreases after the first cycle but then eventually stabilizes and

remains nearly constant in the subsequent cycles. However, for $Ti_3C_2T_x$ the lowest adsorption capacity ($10^{th}$ cycle) can still achieve a value of 439 mg/g, suggesting excellent regeneration stability (Fig. 3.4.b). In aqueous environments, the solvated ammonium ($NH_4^+$) ions have an average radius of 0.331 nm [85], which is smaller than interlayer spacing (0.44 nm) of MXene sheets. The smaller hydrated radius can easily intercalate between the layers without kinetic limitation. Furthermore, with each cycle, the interlayer spacing is likely to increase to a higher value as the lithium ions are removed, which accounts for the increasing adsorption rate (Fig. 3.4.d). The removal of lithium ions lowers site competition making it easier for ammonia to intercalate. The significantly higher value of ammonia adsorption capacity follows the trend of previous studies [82], [87], where 2D materials, particularly graphene, show enhanced adsorption for ammonia compared to sodium chloride (NaCl) desalination. Graphene and graphene oxide (GO) possess similar structural features as MXenes but they lack surface functional groups and the natural hydrophilicity present in all MXenes. It has been established that ammonia interacts via a combination of physisorption and chemisorption [88]. The presence of the −OH and −O functional groups on the $Ti_3C_2T_x$ surface facilitate surface reactions with the $NH_4^+$ ions. The surface chemistry and functional groups affect reactive adsorption as well as physical adsorption mechanisms [88]. In this study, we used a relatively high concentration (500 mg/L) feed solution as a stand-in for wastewater. Higher initial ionic concentrations enhance adsorption capacity [89]. In addition, the use of high concentration feed solution increases current response in the system, which was observed at 30 mA (Fig. 3.5.a). High response current reduces overlap effect and causes an increase in the rate of ion transfer, which positively impacts the capacitance behavior and deionization capacity [90]. First

principle calculations on adsorption behaviors have revealed that $NH_3$ has a very small (more negative) adsorption energy ($E_{ads}$) of -0.078 eV/atom, which results in strong interactions with $Ti_3C_2T_x$ MXenes [33]. The calculations also show high charge transfer ($C_t$ − 0.153 e) between $NH_3$ and $Ti_3C_2T_x$, hence solidifying the hypothesis that the high adsorption capacity is a consequence of chemisorption [33]. Further work is required to understand the kinetics of ammonia adsorption on $Ti_3C_2T_x$ MXenes.

The adsorption rate values for the run are shown in Fig. 3.4.d. The average adsorption rate for AC is significantly lower (0.0021 mg/min/cm$^2$) than $Ti_3C_2T_x$ (0.00545 mg/min/cm$^2$) owing to the lower plateau time and higher deionization efficiency of the later. It is interesting to note that the adsorption rate for AC changes very little across cycles, but it shows an upward trend for $Ti_3C_2T_x$ (not including the first cycle). This is a consequence of decreasing plateau times for $Ti_3C_2T_x$ electrodes. In batch system operation, $C_o$ for each subsequent cycle is different. The value of $C_o$ affects the kinetic accessibility of the dissolved ions, and hence has an effect on the adsorption rate. As discussed earlier, the regeneration efficiency of AC electrodes is marginally higher than $Ti_3C_2T_x$ electrodes (Fig. 3.4.b). This manifests as consistent $C_o$ and resultant adsorption rate for AC.

35
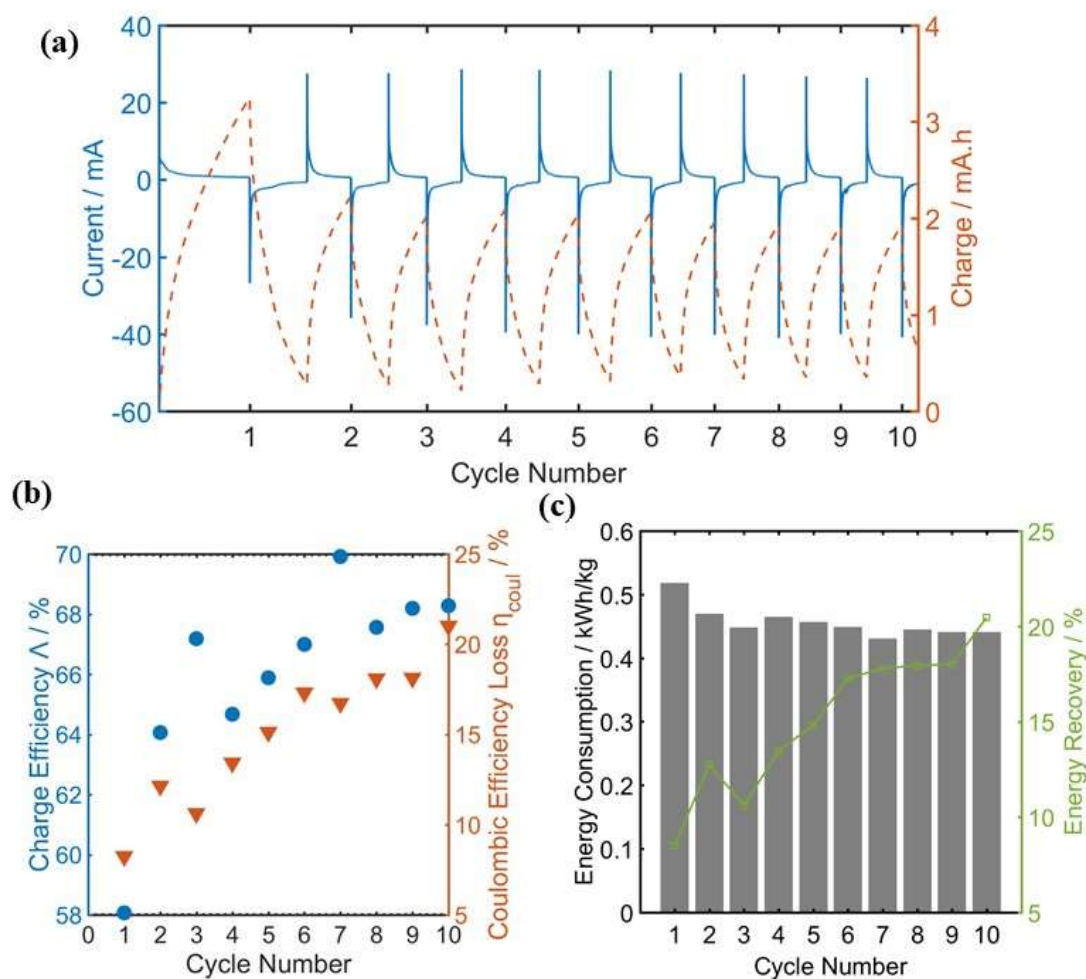


**Figure 3.5.    For each adsorption-desorption cycle: (a) Variation in current and charge; (b) Charge efficiency and Columbic efficiency loss; (c) Energy consumption and recovery.**

The change in the current of the system is consistent with the change in the conductivity of the effluent solution. As shown in Fig. 3.5.a, the cell current decreases and total charge increases as ions are removed from the feed solution. During the discharging step, the current gradually rises back to its initial value, as partial charge is recovered. The charge efficiency ($\Lambda$) and total Coulombic loss ($\eta_{coul}$) in the system (Eq. 5, 6) are shown in Fig. 3.5.b. The values for $\Lambda$ range from 58 to 70% over the course of the CDI test, while

roughly increasing with each subsequent cycle. This is consistent with the observed trend of increasing adsorption rate for each cycle (Fig. 3.4.d), as $\Lambda$ varies with varying $C_o$ [91]. The reported values align well with results reported in literature [92]. A $\Lambda$ value of 100% has never been reported. It has been theorized that the relatively low $\Lambda$ values are an inherent consequence of pseudocapacitive behavior because of the presence of co-ion repulsion and counter-ion adsorption [92]. Some efforts have been made to increase the charge efficiency in CDI systems [93]. However, further work is needed in the area. The charge recovered during the discharging step is lower than the charge transferred during the charging step, resulting in a $\eta_{coul}$ increasing from 8 to 21 % (Eq. 6, Fig. 3.5.b). This is a consequence of leakage current and is typical for supercapacitors and CDI systems. It should also be noted that current increases with each cycle (Fig. 3.5.a), which leads to more pronounced electrode polarization and hence results in an increase in $\eta_{coul}$ with each cycle [62]. Pronounced electrode polarization is also responsible for decreasing deionization capacity (Fig. 3.4.c) [62]. Barring the first cycle, the energy consumption and recovery trends (Fig. 3.5.c) agree with $\eta_{coul}$ and $\Lambda$. This is in line with theoretical studies [93]. Energy recovery is defined as the ratio of recovered energy to consumed energy (Eq. 9). Over the course of ten cycles, 8 to 21% of energy was not recovered by the system. The profile closely resembles $\eta_{coul}$. The average energy consumption for the system was 0.45 kWh/kg. This is higher than the 0.24 kWh/kg obtained by Ma *et al.* [62] using $Ti_3C_2$ films in flow-by CDI for NaCl removal. However, the deionization capacity achieved in this work is significantly higher. Hence, compensating for the marginally higher energy consumption. For comparison, commercial wastewater treatment plants require 4.6 kWh/kg of energy for

ammonium ion removal [94]. This process requires ten times less energy, hence cementing the position of CDI as a green technology.

As shown in Table 3.1., materials such as activated carbon, graphite, and graphene have been studied for ammonia removal in FE-CDI systems [95], [82], [87], [96]. The deionization capacity shows several orders of magnitudes of improvement over 1.5 wt.% graphite [87]. It is apparent that $Ti_3C_2T_x$ MXenes show markedly higher performance for ammonia removal when compared with previously researched electrode materials and systems.

**Table 3.1.    Comparison of performance metrics of different CDI technologies**

| Electrode Material | Ion Species | Cell Architecture | Applied Voltage (V) | Current | Initial Concentration (mg/L) | Deionization Efficiency (%) | Deionization Capacity (mg/g) | Reference |
|---|---|---|---|---|---|---|---|---|
| $Ti_3C_2T_x$ MXene | NaCl | Flow by | 1.2 | Constant Current – 20 mA | 585 | - | 68 | [51] |
| Porous $Ti_3C_2T_x$ MXene | NaCl | Flow by | 1.2 | - | 10000 | - | 45 | [52] |
| $Ti_3C_2T_x$ MXene | NaCl | Flow by | 1.2 | - | 0.085 | - | 13 | [54] |
| Ar-$Ti_3C_2T_x$ MXene | NaCl | Flow by | 0.8 – 1.6 | - | 500 | - | 26.8 | [55] |
| Graphene laminates | $NH_4Cl$ | Membrane Assisted | 2 | 0.17 A | 400 | 99 | 15.3 | [71] |
| Graphite (1.5 wt%) | $NH_4Cl$ | Flow Electrode | 0.2 – 1.2 | - | 20 | 87 | 1.43 | [76] |
| Activated Carbon (0, 2, 5, 10 wt%) | $NH_4^+$–N | Flow Electrode | – 0.8 V | Constant Current – 6 A/m$^2$ | 43 | 95 | - | [85] |
| Carbon Cloth | $NH_4Cl$ | Flow by | 1.2 - 3 | - | 68.8 | 60.5–95.7 | - | [86] |
| **$Ti_3C_2T_x$ MXene** | **$NH_4Cl$** | **Flow Electrode** | **1.2** | **20 – 30 mA** | **500** | **60** | **460** | **This Work** |

### 3.5.    Conclusions

In this study, we demonstrated an FE-CDI system with remarkable ammonia removal performance based on flow electrodes consisting of $Ti_3C_2T_x$ MXene. A high average adsorption capacity of 460 mg/g along with a low energy consumption of 0.45

kWh/kg was witnessed. The results reinforce the strong dependence of FE-CDI performance on the characteristics of the electrode material. Owing to its high conductivity, colloidal stability, high surface area, and unique surface chemistry $Ti_3C_2T_x$ is a promising candidate for ammonia removal and recovery from industrial and commercial wastewaters.

While the results presented are promising, further research, including theoretical modelling of the ammonium ion interaction, kinetic analysis, and testing different MXenes is needed to further improve the process. Due to the nonuniform surface chemistry on MXene surfaces, it is important to consider how different etching approaches will change the adsorption process. Finally, MXenes have been shown as viable for many adsorption processes, but the studies are still in their infancy, $Ti_3C_2T_x$ and other MXenes should be tested for adsorption of more pollutants. However, based on these results, $Ti_3C_2T_x$ is among the most promising environmental remediation materials for ammonia removal from wastewater systems. We expect that the demonstrated work will open new avenues for realizing high performance, energy-efficient, large scale ammonia removal systems.

CHAPTER FOUR: CONLUSIONS

## 4.1.    Outreach

The manuscript in <u>Chapter 3</u>, titled "Removal and Recovery of Ammonia from Wastewater using $Ti_3C_2T_x$ MXene in Flow Electrode Capacitive Deionization" is planned for submission in Royal Society of Chemistry's journal *Energy and Environmental Science* (<u>http://arxiv.org/abs/2007.02853</u>).

An abstract of the results in <u>Chapter 3</u> was submitted and accepted at the *International Conference on Diamond and Carbon Materials 2020.*

U.S. Patent Application Serial No. 62/944,176 was filed based on this work.

## 4.2.    Summary

The research goal of this study was to develop an FE-CDI system with 0.1 wt% $Ti_3C_2T_x$ MXene electrodes for the removal and recovery of ammonium ions from wastewater. A comparative study between 0.1 wt% $Ti_3C_2T_x$ MXenes and 10 wt% AC slurry electrodes was conducted. Comparison between performance parameters of adsorption capacity, ion removal efficiency, regeneration efficiency, energy consumption, and charge efficiency between the two electrode systems, allowed us to confirm our initial hypothesis that higher electrical conductivity, hydrophilicity, colloidal stability, and higher surface area of $Ti_3C_2T_x$ MXenes would likely result in markedly improved performance deionization performance in an FE-CDI system.

Key findings include:

I.     Average adsorption capacity achieved was 460 mg/g

II.     Average energy consumption was 0.45 kWh/kg

III.     System recovered 79% of the initial energy

IV.     Electrodes demonstrated a regeneration stability of 92%

V.     $Ti_3C_2T_x$ MXenes demonstrate a high affinity for ammonia

VI.     $Ti_3C_2T_x$ MXenes in a 1 mg/mL suspension exhibited satisfactory rheological performance when compared against 10 wt% AC suspension.

### 4.3.    Limitations

4.3.1. $Ti_3C_2T_x$ MXenes Oxidation

MXene flakes readily oxidize in the presence of air and moisture. Even though the detailed kinetics of the oxidation process are yet to be unveiled, studies have established that the atomic defects on the $Ti_3C_2$ basal planes act heterogeneous growth sites for conversion to titanium dioxide ($TiO_2$) [97]. The carbon atoms present at titanium vacancies oxidize to form amorphous carbon aggregates. The oxidation of titanium cations occurs at the sites with atomic steps and edges [97]. Uninterrupted exposure of thirty days ends in irreversible degradation to disordered carbon and anatase.

On a macro scale, the rapid oxidation can be visually witnessed by the degradation in color of the black MXene colloidal solution. Studies conducted using UV-Vis spectroscopy demonstrated a correlation between the MXene concentration and visible degradation in an aqueous solution [98]. As oxidation proceeds, the solution also starts to lose its colloidal stability owing to the presence of anatase $TiO_2$.

There have been some research efforts to improve the shelf life of $Ti_3C_2T_x$ MXenes by modifying synthesis processes and/or changes in storage conditions [85].

However, an in-depth understanding of the kinetics of the process is imperative to ensure oxidation resistant $Ti_3C_2T_x$ MXenes.

### 4.3.2 Toxic Synthesis Route

As outlined in Chapter 2.3., the MILD method is a *relatively* safer route for synthesis. However, it still involves the formation of in-situ HF. In addition, MAX phases are prepared from highly flammable powders (e.g. aluminum powder). The presence and use of small, high surface area to volume ratio also increases inhalation and explosion risk. The involves risks make it imperative that only highly trained personnel are allowed to handle the materials and perform the reaction.

### 4.3.3. Mono-ionic System

The adsorption studies in this work were performed using simulated wastewater consisting of a single pollutant at constant concentration. While this allows for ease in laboratory comparisons, it is not representative of real life. Wastewater from any source is usually an amalgamation of various organic and inorganic compounds that vary in concentration over the course of release. The synergistic effects of these compounds on the performance of the system are not yet understood.

### 4.3.4. Economic Analysis

The economics of innovation and market viability are factors that loom over the prospect of large-scale applications of any technology. The lack of a techno-economic analysis limits a practical comparison of this technology against prevalent water remediation techniques.

## 4.4. Future Work

### 4.4.1. Charge Storage Mechanism in $Ti_3C_2T_x$ MXenes

In our hypothesis, we speculated that high capacitance (other studies) and exemplary adsorption capacity (this work) of $Ti_3C_2T_x$ MXenes is a result of a combined effect of the three charge storage mechanism discussed in chap 2.2. While the presence of EDL storage in MXenes is well documented because of their use in pseudocapacitors, the other two charge mechanisms have not been experimentally researched. Hence, the next logical step would be to study the intercalation mechanism via post-operational XRD analysis. If the $NH_4^+$ ions are primarily intercalating between the layers, it would be observable through an increase in interlayer spacing.

In addition, a cyclicvoltammetry analysis to study the electrochemical performance of the electrode slurry will give information about the faradaic reactions, chemisorption, and capacitance mechanism of the electrodes.

Furthermore, a BET analysis will render information about the total surface area of the obtained flakes while an XPS analysis will uncover details about the present surface functional groups. Both of these material properties have a significant role in electrical double layer formation and strength.

### 4.4.2. Multi-ionic System and Scalability

As discussed earlier, a mono-ionic wastewater stream cannot serve as a stand in for actual wastewater. It has been theorized that CDI can be used for targeted ion removal from multi-ionic streams by modifications to ion exchange membranes [99]. Even in their current state, the selectivity of ion exchange membranes is a well understood phenomenon that can be manipulated to only allow the desired ions to pass through [99].

It can be hypothesized that several FE-CDI cells operating in succession can categorically remove (and concentrate) subsequent dissolved impurities. However, it is important to keep note of the fact that a multi-ionic, industrial scale system will readily alter the total charge in the cell which will in turn effect the current in the system [18]. This challenge leads us to believe that a theoretical modeling of the system should be performed before tweaks are made to system design. We plan to use COMSOL electrochemistry and computational fluid dynamics modules to gain a better understanding of the behavior of a comparable industrial scale system.

4.4.3. MXene Compositions

This preliminary study was conducted using the most commonly and widely studied $Ti_3C_2T_x$ MXenes. However, there are nearly 30 different MXenes that have been physically synthesized so far. In particular, niobium (Nb) and Vanadium (V) based MXenes are of particular interest efficient charge-carrier transfer on surfaces and exposed terminal metal sites which promise strong Faradaic/redox activity [100]. In addition, $V_3C_2$ and $Nb_3C_2$ have been studied via DFT analysis to show that their low activation energy barriers make them promising candidates for nitrogen capture and fixation [100]. These exciting studies lead us to hypothesize that V and Nb based MXenes will achieve high adsorption capacity with $NH_4^+$ ion systems. Hence, the next viable step for this work would be the development of scalable synthesis proctocols for the V and Nb based MXenes and their application as FE-CDI electrodes. A comparative study between the more exotic MXenes and the current work on $Ti_3C_2T_x$ MXenes would be of heightened interest.

REFERENCES

[1]     A. Rehman *et al.*, "Economic perspectives of major field crops of Pakistan: An empirical study," *Pacific Sci. Rev. B Humanit. Soc. Sci.*, 2015, doi: 10.1016/j.psrb.2016.09.002.

[2]     A. R. Kalair, N. Abas, Q. Ul Hasan, E. Kalair, A. Kalair, and N. Khan, "Water, energy and food nexus of Indus Water Treaty: Water governance," *Water-Energy Nexus*, 2019, doi: 10.1016/j.wen.2019.04.001.

[3]     Bureau of Economic Analysis, "GDP by Agriculture and Related Industries," 2017. [Online]. Available: https://www.ers.usda.gov/data-products/chart-gallery/gallery/chart-detail/?chartId=58270.

[4]     Idaho State Dept of Agriculture, "Idaho Agriculture Facts and Statistics," 2020. [Online]. Available: https://agri.idaho.gov/main/idaho-agriculture-facts-and-statistics/.

[5]     Environmental Protection Agency, "The Sources and Solutions: Agriculture," 2005. [Online]. Available: https://www.epa.gov/sites/production/files/2015-09/documents/ag_runoff_fact_sheet.pdf.

[6]     Y. Wu, "Indicators for Monitoring Aquatic Ecosystem," in *Periphyton*, 2017.

[7]     R. Singh, "Recycling of Agricultural Waste for Wastewater Treatment," in *Encyclopedia of Renewable and Sustainable Materials*, 2020.

[8]     U.S. EPA, "History of the clean water act," *EPA*. 2015.

[9]     J. W. BLAIR and G. W. MURPHY, "Electrochemical Demineralization of Water with Porous Electrodes of Large Surface Area," 1960.

[10]    K. S. Novoselov *et al.*, "Electric field in atomically thin carbon films," *Science (80-. ).*, 2004, doi: 10.1126/science.1102896.

[11]   M. Inagaki, F. Kang, M. Toyoda, and H. Konno, *Advanced Materials Science and Engineering of Carbon*. 2013.

[12]   M. D. Andelman and G. S. Walker, "Charge barrier flow-through capacitor," US6709560B2, 2004.

[13]   P. Srimuk, X. Su, J. Yoon, D. Aurbach, and V. Presser, "Charge-transfer materials for electrochemical water desalination, ion separation and the recovery of elements," *Nature Reviews Materials*. 2020, doi: 10.1038/s41578-020-0193-1.

[14]   E. García-Quismondo, R. Gómez, F. Vaquero, A. L. Cudero, J. Palma, and M. Anderson, "New testing procedures of a capacitive deionization reactor," *Phys. Chem. Chem. Phys.*, 2013, doi: 10.1039/c3cp50514f.

[15]   W. Tang *et al.*, "Various cell architectures of capacitive deionization: Recent advances and future trends," *Water Research*. 2019, doi: 10.1016/j.watres.2018.11.064.

[16]   S. Il Jeon *et al.*, "Desalination via a new membrane capacitive deionization process utilizing flow-electrodes," *Energy Environ. Sci.*, 2013, doi: 10.1039/c3ee24443a.

[17]   A. Rommerskirchen, B. Ohs, K. A. Hepp, R. Femmer, and M. Wessling, "Modeling continuous flow-electrode capacitive deionization processes with ion-exchange membranes," *J. Memb. Sci.*, 2018, doi: 10.1016/j.memsci.2017.10.026.

[18]   S. Porada, R. Zhao, A. Van Der Wal, V. Presser, and P. M. Biesheuvel, "Review on the science and technology of water desalination by capacitive deionization," *Progress in Materials Science*. 2013, doi: 10.1016/j.pmatsci.2013.03.005.

[19]   W. Xing *et al.*, "Versatile applications of capacitive deionization (CDI)-based technologies," *Desalination*, vol. 482, p. 114390, 2020, doi: https://doi.org/10.1016/j.desal.2020.114390.

[20]   C. Choi *et al.*, "Achieving high energy density and high power density with pseudocapacitive materials," *Nature Reviews Materials*. 2020, doi: 10.1038/s41578-019-0142-z.

[21]   G. M. Torrie and J. P. Valleau, "Electrical double layers. 4. Limitations of the

Gouy-Chapman theory," *J. Phys. Chem.*, 1982, doi: 10.1021/j100213a035.

[22] "Reference Module in Chemistry, Molecular Sciences and Chemical Engineering," *Choice Rev. Online*, 2014, doi: 10.5860/choice.51-6506.

[23] S. Zhang, T. Ma, A. Erdemir, and Q. Li, "Tribology of two-dimensional materials: From mechanisms to modulating strategies," *Materials Today*. 2019, doi: 10.1016/j.mattod.2018.12.002.

[24] B. Anasori, M. R. Lukatskaya, and Y. Gogotsi, "2D metal carbides and nitrides (MXenes) for energy storage," *Nature Reviews Materials*. 2017, doi: 10.1038/natrevmats.2016.98.

[25] Y. Gogotsi and B. Anasori, "The Rise of MXenes," *ACS Nano*. 2019, doi: 10.1021/acsnano.9b06394.

[26] C. Yang *et al.*, "Flexible Nitrogen-Doped 2D Titanium Carbides (MXene) Films Constructed by an Ex Situ Solvothermal Method with Extraordinary Volumetric Capacitance," *Adv. Energy Mater.*, 2018, doi: 10.1002/aenm.201802087.

[27] M. Magnuson and M. Mattesini, "Chemical bonding and electronic-structure in MAX phases as viewed by X-ray spectroscopy and density functional theory," *Thin Solid Films*. 2017, doi: 10.1016/j.tsf.2016.11.005.

[28] M. Naguib *et al.*, "Two-Dimensional Nanocrystals: Two-Dimensional Nanocrystals Produced by Exfoliation of Ti3AlC2 (Adv. Mater. 37/2011)," *Adv. Mater.*, 2011, doi: 10.1002/adma.201190147.

[29] P. Nayak, Q. Jiang, R. Mohanraman, D. Anjum, M. N. Hedhili, and H. N. Alshareef, "Inherent electrochemistry and charge transfer properties of few-layered two-dimensional Ti3C2Tx MXene," *Nanoscale*, 2018, doi: 10.1039/c8nr01883a.

[30] C. E. Shuck *et al.*, "Scalable Synthesis of Ti3C2Tx MXene," *Adv. Eng. Mater.*, vol. 22, no. 3, p. 1901241, 2020, doi: 10.1002/adem.201901241.

[31] L. Verger, C. Xu, V. Natu, H. M. Cheng, W. Ren, and M. W. Barsoum, "Overview of the synthesis of MXenes and other ultrathin 2D transition metal carbides and

nitrides," *Current Opinion in Solid State and Materials Science*. 2019, doi: 10.1016/j.cossms.2019.02.001.

[32]    W. H. Bragg, "The intensity of reflexion of X- rays by crystals," *Acta Crystallogr. Sect. A*, 1969, doi: 10.1107/S0567739469000039.

[33]    M. Wu *et al.*, "Ti3C2 MXene-Based Sensors with High Selectivity for NH3 Detection at Room Temperature," *ACS Sensors*, 2019, doi: 10.1021/acssensors.9b01308.

[34]    M. R. Lukatskaya *et al.*, "Ultra-high-rate pseudocapacitive energy storage in two-dimensional transition metal carbides," *Nat. Energy*, 2017, doi: 10.1038/nenergy.2017.105.

[35]    J. Macknick, R. Newmark, G. Heath, and K. C. Hallett, "Operational water consumption and withdrawal factors for electricity generating technologies: A review of existing literature," *Environ. Res. Lett.*, 2012, doi: 10.1088/1748-9326/7/4/045802.

[36]    DOE, "Energy demands on water resources," 2006.

[37]    I. E. A. IEA, "World Energy Outlook 2019 – Analysis - IEA," *World Energy Outlook 2019*, 2019. .

[38]    M. Palo, J. Uusivuori, G. Mery, A. V. Korotkov, and D. Humphreys, "World Forests, Markets and Policies: Towards a Balance," 2001.

[39]    C. Coyette, H.; Schenk, *Agriculture, forestry and fishery statistics*. 2019.

[40]    U.S Geological Survey, *Mineral Commodity Summaries 2020*. 2020.

[41]    W. J. Visek, "Ammonia: Its Effects on Biological Systems, Metabolic Hormones, and Reproduction," *J. Dairy Sci.*, 1984, doi: 10.3168/jds.S0022-0302(84)81331-4.

[42]    N. Gruber and J. N. Galloway, "An Earth-system perspective of the global nitrogen cycle," *Nature*. 2008, doi: 10.1038/nature06592.

[43]    R. R. Karri, J. N. Sahu, and V. Chimmiri, "Critical review of abatement of ammonia from wastewater," *Journal of Molecular Liquids*. 2018, doi:

10.1016/j.molliq.2018.03.120.

[44]    F. Jaramillo, M. Orchard, C. Muñoz, M. Zamorano, and C. Antileo, "Advanced strategies to improve nitrification process in sequencing batch reactors - A review," *Journal of Environmental Management*. 2018, doi: 10.1016/j.jenvman.2018.04.019.

[45]    R. Semiat, "Energy issues in desalination processes," *Environmental Science and Technology*. 2008, doi: 10.1021/es801330u.

[46]    A. W. W. Association, *Reverse Osmosis and Nanofiltration (M46): AWWA Manual of Practice*, Second. 2007.

[47]    M. A. Ahmed and S. Tewari, "Capacitive deionization: Processes, materials and state of the technology," *Journal of Electroanalytical Chemistry*. 2018, doi: 10.1016/j.jelechem.2018.02.024.

[48]    K. Tang, Y.-H. Kim, S. Yiacoumi, and C. Tsouris, "(Invited) Capacitive Deionization of High-Salinity Water Using Ion-Exchange Membranes," *{ECS} Meet. Abstr.*, 2017, doi: 10.1149/ma2017-02/22/1032.

[49]    F. A. AlMarzooqi, A. A. Al Ghaferi, I. Saadat, and N. Hilal, "Application of Capacitive Deionisation in water desalination: A review," *Desalination*. 2014, doi: 10.1016/j.desal.2014.02.031.

[50]    Y. Oren, "Capacitive deionization (CDI) for desalination and water treatment - past, present and future (a review)," *Desalination*, 2008, doi: 10.1016/j.desal.2007.08.005.

[51]    P. M. Biesheuvel, B. van Limpt, and A. van der Wal, "Dynamic Adsorption/Desorption Process Model for Capacitive Deionization," *J. Phys. Chem. C*, vol. 113, no. 14, pp. 5636–5640, Apr. 2009, doi: 10.1021/jp809644s.

[52]    E. M. Remillard, A. N. Shocron, J. Rahill, M. E. Suss, and C. D. Vecitis, "A direct comparison of flow-by and flow-through capacitive deionization," *Desalination*, 2018, doi: 10.1016/j.desal.2018.01.018.

[53]    S. Dahiya and B. K. Mishra, "Enhancing understandability and performance of

flow electrode capacitive deionisation by optimizing configurational and operational parameters: A review on recent progress," *Separation and Purification Technology*. 2020, doi: 10.1016/j.seppur.2020.116660.

[54]    P. Ratajczak, M. E. Suss, F. Kaasik, and F. Béguin, "Carbon electrodes for capacitive technologies," *Energy Storage Mater.*, vol. 16, pp. 126–145, 2019, doi: https://doi.org/10.1016/j.ensm.2018.04.031.

[55]    M. A. Luciano, H. Ribeiro, G. E. Bruch, and G. G. Silva, "Efficiency of capacitive deionization using carbon materials based electrodes for water desalination," *J. Electroanal. Chem.*, vol. 859, p. 113840, 2020, doi: https://doi.org/10.1016/j.jelechem.2020.113840.

[56]    K. Y. Choo, C. Y. Yoo, M. H. Han, and D. K. Kim, "Electrochemical analysis of slurry electrodes for flow-electrode capacitive deionization," *J. Electroanal. Chem.*, 2017, doi: 10.1016/j.jelechem.2017.10.040.

[57]    G. Deysher *et al.*, "Synthesis of Mo4VAlC4 MAX Phase and Two-Dimensional Mo4VC4 MXene with Five Atomic Layers of Transition Metals," *ACS Nano*, 2020, doi: 10.1021/acsnano.9b07708.

[58]    K. Maleski, V. N. Mochalin, and Y. Gogotsi, "Dispersions of Two-Dimensional Titanium Carbide MXene in Organic Solvents," *Chem. Mater.*, 2017, doi: 10.1021/acs.chemmater.6b04830.

[59]    Y. Zhang, L. Wang, N. Zhang, and Z. Zhou, "Adsorptive environmental applications of MXene nanomaterials: A review," *RSC Advances*. 2018, doi: 10.1039/c8ra03077d.

[60]    G. Liu *et al.*, "Ultrathin two-dimensional MXene membrane for pervaporation desalination," *J. Memb. Sci.*, 2018, doi: 10.1016/j.memsci.2017.11.065.

[61]    G. K. Nasrallah, M. Al-Asmakh, K. Rasool, and K. A. Mahmoud, "Ecotoxicological assessment of Ti3C2T:X (MXene) using a zebrafish embryo model," *Environ. Sci. Nano*, 2018, doi: 10.1039/c7en01239j.

[62]    J. Ma, Y. Cheng, L. Wang, X. Dai, and F. Yu, "Free-standing Ti3C2Tx MXene

film as binder-free electrode in capacitive deionization with an ultrahigh desalination capacity," *Chem. Eng. J.*, 2020, doi: 10.1016/j.cej.2019.123329.

[63]    W. Bao *et al.*, "Porous Cryo-Dried MXene for Efficient Capacitive Deionization," *Joule*, 2018, doi: 10.1016/j.joule.2018.02.018.

[64]    L. Agartan *et al.*, "Influence of operating conditions on the desalination performance of a symmetric pre-conditioned Ti3C2Tx-MXene membrane capacitive deionization system," *Desalination*, vol. 477, p. 114267, 2020, doi: https://doi.org/10.1016/j.desal.2019.114267.

[65]    P. Srimuk *et al.*, "MXene as a novel intercalation-type pseudocapacitive cathode and anode for capacitive deionization," *J. Mater. Chem. A*, 2016, doi: 10.1039/c6ta07833h.

[66]    L. Guo, X. Wang, Z. Y. Leong, R. Mo, L. Sun, and H. Y. Yang, "Ar plasma modification of 2D MXene Ti3C2Tx nanosheets for efficient capacitive desalination," *FlatChem*, 2018, doi: 10.1016/j.flatc.2018.01.001.

[67]    S. Venkateshalu and A. N. Grace, "MXenes—A new class of 2D layered materials: Synthesis, properties, applications as supercapacitor electrode and beyond," *Applied Materials Today*. 2020, doi: 10.1016/j.apmt.2019.100509.

[68]    Y. Y. Peng *et al.*, "All-MXene (2D titanium carbide) solid-state microsupercapacitors for on-chip energy storage," *Energy Environ. Sci.*, 2016, doi: 10.1039/c6ee01717g.

[69]    X. Zhang, Z. Zhang, and Z. Zhou, "MXene-based materials for electrochemical energy storage," *Journal of Energy Chemistry*. 2018, doi: 10.1016/j.jechem.2017.08.004.

[70]    A. K. Shukla, A. Banerjee, M. K. Ravikumar, and A. Jalajakshi, "Electrochemical capacitors: Technical challenges and prognosis for future markets," *Electrochimica Acta*. 2012, doi: 10.1016/j.electacta.2012.03.059.

[71]    P. Simon and Y. Gogotsi, "Materials for electrochemical capacitors," *Nature Materials*. 2008, doi: 10.1038/nmat2297.

[72] R. Malik, "Maxing Out Water Desalination with MXenes," *Joule*. 2018, doi: 10.1016/j.joule.2018.04.001.

[73] Y. Zhao, Y. Wang, R. Wang, Y. Wu, S. Xu, and J. Wang, "Performance comparison and energy consumption analysis of capacitive deionization and membrane capacitive deionization processes," *Desalination*. 2013, doi: 10.1016/j.desal.2013.06.009.

[74] K. Maleski, C. E. Ren, M. Q. Zhao, B. Anasori, and Y. Gogotsi, "Size-Dependent Physical and Electrochemical Properties of Two-Dimensional MXene Flakes," *ACS Appl. Mater. Interfaces*, 2018, doi: 10.1021/acsami.8b04662.

[75] C. E. Shuck *et al.*, "Effect of Ti3AlC2 MAX Phase on Structure and Properties of Resultant Ti3C2Tx MXene," *ACS Appl. Nano Mater.*, 2019, doi: 10.1021/acsanm.9b00286.

[76] S. A. Hawks *et al.*, "Performance metrics for the objective assessment of capacitive deionization systems," *Water Research*. 2019, doi: 10.1016/j.watres.2018.10.074.

[77] K. Singh, S. Porada, H. D. de Gier, P. M. Biesheuvel, and L. C. P. M. de Smet, "Timeline on the application of intercalation materials in Capacitive Deionization," *Desalination*. 2019, doi: 10.1016/j.desal.2018.12.015.

[78] M. Lu, W. Han, H. Li, W. Zhang, and B. Zhang, "There is plenty of space in the MXene layers: The confinement and fillings," *J. Energy Chem.*, 2020, doi: 10.1016/j.jechem.2020.02.032.

[79] A. Sarycheva and Y. Gogotsi, "Raman Spectroscopy Analysis of the Structure and Surface Chemistry of Ti3C2Tx MXene," *Chem. Mater.*, vol. 32, no. 8, pp. 3480–3488, Apr. 2020, doi: 10.1021/acs.chemmater.0c00359.

[80] M. N. Rahaman, *Ceramic processing*. 2017.

[81] K. Fang, H. Gong, W. He, F. Peng, C. He, and K. Wang, "Recovering ammonia from municipal wastewater by flow-electrode capacitive deionization," *Chem. Eng. J.*, 2018, doi: 10.1016/j.cej.2018.04.128.

[82] Y. Wimalasiri, M. Mossad, and L. Zou, "Thermodynamics and kinetics of adsorption of ammonium ions by graphene laminate electrodes in capacitive deionization," *Desalination*, 2015, doi: 10.1016/j.desal.2014.11.015.

[83] X. Sang *et al.*, "Atomic defects in monolayer titanium carbide (Ti3C2Tx) MXene," *ACS Nano*, 2016, doi: 10.1021/acsnano.6b05240.

[84] T. Habib *et al.*, "Oxidation stability of Ti3C2Tx MXene nanosheets in solvents and composite films," *npj 2D Mater. Appl.*, 2019, doi: 10.1038/s41699-019-0089-3.

[85] Y. Lee *et al.*, "Oxidation-resistant titanium carbide MXene film," *J. Mater. Chem. A*, 2019, doi: 10.1039/C9TA07036B.

[86] V. Natu, R. Pai, M. Sokol, M. Carey, V. Kalra, and M. W. Barsoum, "2D Ti3C2Tz MXene Synthesized by Water-free Etching of Ti3AlC2 in Polar Organic Solvents," *Chem*, 2020, doi: 10.1016/j.chempr.2020.01.019.

[87] M. Seredych and T. J. Bandosz, "Removal of ammonia by graphite oxide via its intercalation and reactive adsorption," *Carbon*. 2007, doi: 10.1016/j.carbon.2007.06.007.

[88] S. Wang, H. Sun, H. M. Ang, and M. O. Tadé, "Adsorptive remediation of environmental pollutants using novel graphene-based nanomaterials," *Chemical Engineering Journal*. 2013, doi: 10.1016/j.cej.2013.04.070.

[89] D. Moreno and M. C. Hatzell, "Influence of Feed-Electrode Concentration Differences in Flow-Electrode Systems for Capacitive Deionization," *Ind. Eng. Chem. Res.*, 2018, doi: 10.1021/acs.iecr.8b01626.

[90] Y. Li *et al.*, "A protic salt-derived porous carbon for efficient capacitive deionization: Balance between porous structure and chemical composition," *Carbon N. Y.*, 2017, doi: 10.1016/j.carbon.2017.01.084.

[91] P. M. Biesheuvel, S. Porada, M. Levi, and M. Z. Bazant, "Attractive forces in microporous carbon electrodes for capacitive deionization," *J. Solid State Electrochem.*, 2014, doi: 10.1007/s10008-014-2383-5.

[92] T. Kim, J. E. Dykstra, S. Porada, A. van der Wal, J. Yoon, and P. M. Biesheuvel, "Enhanced charge efficiency and reduced energy use in capacitive deionization by increasing the discharge voltage," *J. Colloid Interface Sci.*, 2015, doi: 10.1016/j.jcis.2014.08.041.

[93] X. Gao, A. Omosebi, J. Landon, and K. Liu, "Enhancement of charge efficiency for a capacitive deionization cell using carbon xerogel with modified potential of zero charge," *Electrochem. commun.*, 2014, doi: 10.1016/j.elecom.2013.12.004.

[94] M. Ekman, B. Björlenius, and M. Andersson, "Control of the aeration volume in an activated sludge process using supervisory control strategies," *Water Res.*, 2006, doi: 10.1016/j.watres.2006.02.019.

[95] C. Zhang, J. Ma, and T. D. Waite, "Ammonia-Rich Solution Production from Wastewaters Using Chemical-Free Flow-Electrode Capacitive Deionization," *ACS Sustain. Chem. Eng.*, 2019, doi: 10.1021/acssuschemeng.9b00314.

[96] Z. Ge, X. Chen, X. Huang, and Z. J. Ren, "Capacitive deionization for nutrient recovery from wastewater with disinfection capability," *Environ. Sci. Water Res. Technol.*, 2018, doi: 10.1039/c7ew00350a.

[97] Y. Chae *et al.*, "An investigation into the factors governing the oxidation of two-dimensional Ti 3 C 2 MXene," *Nanoscale*, 2019, doi: 10.1039/c9nr00084d.

[98] C. J. Zhang *et al.*, "Oxidation Stability of Colloidal Two-Dimensional Titanium Carbides (MXenes)," *Chem. Mater.*, 2017, doi: 10.1021/acs.chemmater.7b00745.

[99] Khoiruddin, D. Ariono, Subagjo, and I. G. Wenten, "Surface modification of ion-exchange membranes: Methods, characteristics, and performance," *Journal of Applied Polymer Science*. 2017, doi: 10.1002/app.45540.

[100] L. lan Yu, J. zhou Qin, W. jun Zhao, Z. guang Zhang, J. Ke, and B. jun Liu, "Advances in Two-Dimensional MXenes for Nitrogen Electrocatalytic Reduction to Ammonia," *International Journal of Photoenergy*. 2020, doi: 10.1155/2020/5251431.